LOCAL SITE RESPONSE IN SAN SALVADOR, EL SALVADOR: COMPARISON BETWEEN MICROTREMORS, WEAK MOTION AND STRONG MOTION

Kuvvet Atakan[1], Mauricio Ciudad Real[2], Rodolfo Torres[2]
Juan Carlos Figueroa[2], Roberto Arias[2], and Pedro Santos[2]

(1) *Institute of Solid Earth Physics, University of Bergen, Bergen, Norway.*
(2) *Centro de Investigaciones Geotécnicas, San Salvador, El Salvador, C.A.*

ABSTRACT

The San Salvador area lies along the Central American volcanic chain, which is the product of the northeast-directed subduction of the Cocos plate beneath the Caribbean plate. The destructive earthquakes occurred in El Salvador during the last few decades, originate basically from shallow, moderate sized earthquakes with epicenters falling into the volcanic zone. The most recent one of these, the Oct.10, 1986 earthquake (M_S=5.4) caused considerable damage to the city of San Salvador with more than 1500 casualties and about 10,000 injured. The material losses reached up to USD 1,5 billion. In order to improve seismic design code, factors such as the local site response has to be taken into account. Present study intends to demonstrate the applicability and the limitations of the different techniques through a comparison between three data sets from, microtremors, weak motion and strong motion.

Data from four sites within the metropolitan area are used to investigate the local site response in San Salvador. Spectral ratios of the horizontal components from the four sedimentary sites with respect to a reference site, are calculated and compared between the records of one minute duration background noise (microtremors), earthquakes from the subduction zone (weak motion) and the earthquake of Oct.10, 1986 (strong motion). Results indicate site amplifications ranging from 3-9 at all sites on all three data sets within the frequency band 1.0-10.0 Hz. However, within this frequency band, no correlation is found at any dominant frequency. This is probably due to the variations in the thicknesses and the properties of the sedimentary layers both vertically and laterally. Average amplification factors obtained from the three data sets show a trend indicating a gradual decrease from microtremors to weak and to strong motion. Estimates on all four sites indicate higher values (5.1-8.5) for microtremors compared to the weak motion data (4.5-6.8), whereas strong motion data shows the lowest amplification factors (3.3-4.5). In order to obtain reliable estimates of site amplification, this nonlinearity between the three data sets have to be taken into account. Unless calibrated with the strong motion data, caution is recommended in using microtremors.

INTRODUCTION:

Any reliable estimation of seismic hazard, is largely dependent on the detailed information of the local site response. This phenomenon has been recognized for some time *(e.g. Milne, 1898)*. In order to determine the site response, several methods are used, that can be categorized into two major groups, the theoretical (analytical) and the empirical methods. The theoretical calculation of the site response, mainly based on the inversion techniques, basically require a very good knowledge of the geotechnical parameters to constrain the results. Depending on the type of inversion used, several assumptions have to be made regarding the shape of the source spectrum or the site response at the selected stations. Empirical methods are somehow more effective in the sense that they are based on calculating the frequency spectrum directly from the recorded ground motion. Among the empirical methods, the spectral ratio of a sedimentary site with respect to a bedrock reference site is becoming widely used in recent years *(e.g. Borcherdt, 1970; Borcherdt and Gibbs, 1976; Rogers et al., 1984)*. Effective use of this technique is demonstrated at different sites and geological conditions following the large destructive earthquakes during the last decade *(e.g. Singh et al., 1988; Lermo et al., 1988; Borcherdt et al., 1989; Hough et al., 1990)*. Some review papers, discuss the effectiveness of the different methods used in the site response estimate *(e.g. Aki, 1988; Hartzell, 1992; Aki, 1993)*. New methods were also introduced recently, based on using only one-station recordings (horizontal vs. vertical components) *(Nakamura, 1989; Lermo and Chávez-García, 1993)*, and on the cross-spectrum estimate *(Şafak, 1991; Field et al., 1992)*.

The destructive earthquakes experienced in El Salvador during the last few decades, originate basically from the shallow, moderate sized earthquakes with epicenters falling in to the volcanic zone. The most recent one of these, the Oct.10, 1986 earthquake (M_S=5.4) caused a considerable damage to the city of San Salvador with more than 1500 casualties and about 10,000 injured *(Olson, 1987)*. The material losses reached up to USD 1,5 billion. Much of this damage was related to the local site conditions *(Atakan and Torres, 1993)*. The present study intends to demonstrate the applicability and the limitations of the spectral ratio technique used in estimating the local site response, through a comparison between three data sets from, microtremors, weak and strong ground motion.

In this study, we have used background noise measurements of one minute duration from the selected five sites where there are permanent accelerograph stations, Centro de Investigaciones Geotécnicas (CIG), Instituto Geográfico Nacional (IGN), Universidad Centro Americana (UCA), Hotel Camino Real (HCR) and Hotel Sheraton (SHE) *(Figure 1)*. In addition, two other sites at the western flank of the San Jacinto Hill (SJA and SOC) are used as bedrock reference sites. The spectral ratios from these are compared with data collected from the subduction zone earthquakes recorded at the same sites. These two data sets are then correlated with the strong motion records of the Oct.10, 1986 earthquake.

GEOLOGICAL SETTING:

The San Salvador area lies along the axis of the Central American volcanic chain, which is the product of the northeast-directed subduction of the Cocos plate beneath the Caribbean plate with an absolute plate motion of 8.0 cm/year *(Rymer, 1987; Weinberg, 1992)*. The plate-tectonic framework of the Central America and the Caribbean was previously reviewed by several authors *(e.g. Molnar and Sykes, 1969; Malfait and Dinkelmann, 1972; Burke et al., 1984; Mann and Burke, 1984; Dengo, 1985)*. The generalized geological overview of El Salvador was discussed by Wiesemann *(1975)*, and later the geological map was published by Weber et al. *(1978)*.

The metropolitan area of San Salvador is underlain by middle and upper Cenozoic volcanic and volcanoclastic deposits of different origin, mainly derived from the adjacent volcanoes *(Weber et al., 1978)*. The area lies on the gentle eastern slope of the San Salvador volcano dissected by deeply incised streams and rivers *(Figure 2a)*, and is surrounded by four major volcanic features. These are; the San Salvador volcano, with a minor cinder cone in its center to the west-northwest; the Cerros de Mariona to the north; a collapsed caldera, lake Ilopango to the east; and an inactive volcanic dome with a minor parasitic cone, Cerro San Jacinto to the south-southeast *(Figure 3)*.

Relevant to the local site response, there are two major deposits forming part of the San Salvador Formation that cover the metropolitan area. These are, the youngest unit Holocene volcanic ashes, locally named as *"tierra blanca"* because of its light colour, and the underlying Pleiostecene aged, browned coloured tuffs *(Scmidt-Thomé, 1975)*. The latter unit is as thick as 25 m and is derived from the San Salvador volcano, whereas the younger unit,

is approximately 25 m thick immediately underneath the city and may reach up to 50 m towards the lake Ilopango *(Rymer, 1987)*. This younger unit represents multiple eruptions from the former Ilopango volcano. The characteristics of the uppermost 10 to 30 m of these sediments, are revealed in either geotechnical investigations or in cross sections outcropping along the river banks. The clast compositions and the grain sizes vary considerably within short distances as well as the thicknesses. The degree of consolidation is another characteristic feature varying considerably as indicated by the penetration tests *(Figure 2b)*.

There are three major fault trends in the area, in NNE-SSW/N-S, NE-SW and NW-SE *(Durr et al., 1960)*. In addition, the fourth and the oldest trend can be inferred from the general strike direction of the volcanic chain in the WNW-ESE/E-W direction *(Rymer, 1987)*. Among the other three, the north-south trending faults are less distinct and occur only locally *(Rymer, 1987)*. The youngest faults are the dominant trend in the NE-SW and the conjugate set in the NW-SE directions. All faults seem to have steep dip angles generally larger than 65° and appear active *(Schmidt-Thomé, 1975)*. Although the individual fault trends may have developed at different times, they have been repeatedly reactivated. The reactivation of the NNE-SSW trending fault during the October 10, 1986 earthquake is the most recent example *(Figure 3) (White et al.,1987; Harlow et al.,1993)*.

SEISMICITY:

In El Salvador, as well as in most Central American countries, the main cause of seismic activity is the subduction of the Cocos plate under the Caribbean plate with an average velocity of 8 cm/yr *(Weinberg, 1992)*. Around 80% of the seismic activity in El Salvador has its origin in the subduction zone. The other 20% is generated either by local fault movements or volcanic activity.

The city of San Salvador has experienced several destructive earthquakes within this century *(Figure 4)*. The most damaging were; on June 8, 1917, where two almost consecutive events with magnitudes 6.4 and 6.3 (M_S) occurred respectively, followed by an eruption half an hour later; on April 27, 1919 (M_S=6.0); and on May 3, 1965 (M_S=6.0), where it was preceeded by an unusual number of shocks (more than 8000) *(White et al., 1987)*. Although the epicenter of the latter is close to the October 10, 1986 earthquake, the casualties were much lower due to the high number of foreshocks which alerted the population. Even though the earthquakes ocurring in the subduction zone have larger magnitudes than the ones

occurring inland, they are less destructive. This is mainly due to the relative larger epicentral distances and deeper focal depths. As in the case of El Salvador, the most destructive earthquakes in Central America have been inland earthquakes related to the volcanic zone. Among them, December 23, 1972 earthquake in Nicaragua (M_S=6.2; NEIS), April 14, 1973 in Costa Rica (M_S=6.5; NEIS), February 4,1976 in Guatemala (M_S=7.5; NEIS) and October 10, 1986 in El Salvador (M_S=5.4; NEIC) have caused considerable damage and a high number of casualties *(White et al., 1987; White and Harlow, 1993; Harlow et.al., 1993).*

The main shock of the October 10, 1986 earthquake reached intensities as high as IX on the Modified Mercalli intensity scale mainly in the area along the fault plane striking NNE-SSW *(Alvarez, 1987) (Figure 5).* The highest intensities also correspond to the central and densely populated part of the city. *Figure 5* shows the distribution of damage with increasing degree of intensity, as well as the macroseismic intensity contours. The shallow depth of the mainshock resulted in high damage concentrated in a relatively narrow zone. This, combined with the fact that most of the damage to buildings was the result of poor construction practices, have lead to a large number of casualties *(Olson, 1987).*

DATA SETS:

Three different data sets were collected from the four sedimentary sites CIG, IGN, UCA and HCR. These are the microtremors, weak ground motion from the subduction zone earthquakes and strong ground motion data from the Oct.10, 1986 earthquake. In addition, the pre-event noise windows from the weak motion data were used as the fourth data set to compare with the microtremors recorded randomly.

The strong motion data set was collected by the permanent accelerograph network operated by Centro de Investigaciones Geotécnicas (CIG). Data from CIG, IGN, UCA and HCR, recorded by the Kinemetrics SMA-1 instruments, were available. Recordings from the SHE station was used as the reference site for the strong motion data, because of its proximity to the bedrock outcrops. For the other data sets, the reference site SJA located on the western flank of the San Jacinto dome, was used. In addition, another reference site, SOC (close to SJA) was used in some of the earthquake recordings. The combinations used for spectral ratios for different data sets are listed in *Table I.* The SJA station was used as a standard reference and the other reference sites were corrected accordingly.

Because of the limitations in the number of instruments used for the microtremor and the weak motion recordings, only a pair of data at a time, simultaneously taken at a sedimentary and a bedrock reference site, were collected. The strong motion records, on the other hand, were taken simultaneously at all five sites. For the microtremors, background noise measurements of one minute duration were collected from each site, using Kinemetrics SSR-1 digital recording systems. Six such windows, with a sampling rate of 100, were recorded, and among them the best records, in terms of the data quality, were chosen for the analysis. Simultaneous measurements were also taken both inside the buildings and outside in the free-field, which showed similar results. In order to have a more uniform data set, only the measurements taken inside the buildings, where the permanent strong motion instruments were installed, were used in the analysis.

The weak motion data is chosen among the 16 events recorded. Only those events which had similar locations and magnitudes were used in the analysis. The epicenter locations of the 16 events are shown in *Figure 6 (see also Table II).*

Spectral ratios of the four sedimentary sites with respect to the bedrock reference site are calculated for all four data sets. For each pair of data, the spectra are computed on windows with same durations (i.e. same number of samples) chosen at the S-wave part of the signal including the S-wave coda (beleived to give similar amplifications *e.g. Gutierrez and Singh, 1993*). The signals were cosine tapered and Fourier transformed (with Fast Fourier Transformations). The spectral amplitudes were then smoothed with one-third octave band filter.

MICROTREMORS:

Spectral ratios of the four sedimentary sites with respect to the reference site SJA were calculated and the results are presented in *Figures 7 & 8*, for the N-S and E-W components respectively. The spectral amplifications are observed at all sites, along a broad frequency range. Within 1.0 to 10.0 Hz, the amplifications reach upto 10-15, with peak amplifications between 2.0 to 3.0 Hz., gradually decreasing down to a factor of 2.0 at about 4.0-5.0 Hz. This phenomenon is observed at all sites, except for UCA, where there is a deamplification between 8.0 to 25.0 Hz. For frequencies lower than 1.0 Hz, we do not beleive we have enough resolution for interpreting any behavior. The maximum amplifications are 10.5

(3.0Hz) at CIG, 17.0 (2.0Hz) at IGN, 11.0 (2.4Hz) at UCA and 12.0 (2.5Hz) at HCR. The corresponding average values for four sites are 6.4 for CIG, 8.5 for IGN, 6.4 for UCA and 6.0 for HCR.

For the E-W components, the records from IGN are missing due to instrumental problems. The other three sites show lower and more irregular amplification patterns within the frequency range 1.0 to 10.0 Hz. The maximum amplifications are at CIG 9.0 (8.4Hz), UCA 4.2 (3.5Hz) and HCR 5.1 (7.2Hz). Average amplication factors are 4.6 for CIG, 3.9 for UCA and 4.1 for HCR.

Average of N-S and E-W components are also calculated for the maximum and the average amplification factors. The maximum amplifications show 9.8 for CIG, 17.0 for IGN (only N-S), 7.6 for UCA and 8.5 for HCR. The average amplification factors indicate, on the other hand, 5.5 for CIG, 8.5 for IGN, 5.1 for UCA and 5.1 for HCR.

PRE-EVENT NOISE RECORDS:

The pre-event windows of 30 seconds duration from the earthquake records used for the weak motion data set, are used for comparison with the microtremor measurements. The results are presented in *Figures 9 and 10*, for the N-S and E-W components respectively. At all sites spectral amplifications are observed within the frequency range 1.0 to 10.0 Hz. For the N-S components, the maximum amplifications observed on the four sites are 27.0 (4.9Hz) at CIG, 20.0 (2.4Hz) at IGN, 21.0 (3.5Hz) at UCA and 6.2 (2.4Hz) at HCR. The average amplification factors are 10.4 for CIG, 11.1 for IGN, 6.0 for UCA and 5.5 for HCR.

The E-W components show somewhat lower values of amplifications. The maximum amplification factors are for CIG 11.0 (4.0Hz), IGN 14.1 (7.0Hz) and HCR 8.4 (10.0Hz). Here, the records from UCA are missing due to instrumental problems. The average amplification factors for the same stations are 7.8 for CIG, 10.1 for IGN and 6.2 for HCR.

Average of N-S and E-W components are also calculated for the maximum and the average amplification factors. The maximum amplifications show 19.0 for CIG, 17.0 for IGN, 21.0 for UCA (only N-S component), and 7.3 for HCR. The average amplification factors indicate, on the other hand, 9.1 for CIG, 10.6 for IGN, 6.0 for UCA and 5.9 for HCR.

WEAK MOTION:

Weak motion records are chosen among the 16 earthquakes located along the subduction zone in the south. The events used in the analysis are listed in *Table II.* In general spectral amplifications are observed on all records within a wide range of frequencies. At higher frequencies (usualluly above 10.0 Hz), the phenomenon is reversed giving de-amplifications.

For the N-S components *(Figure 11)*, the spectral ratios of four sedimentary sites with respect to the bedrock reference site indicate maximum amplifications of 8.5 (2.1Hz) for CIG, 16.0 (2.9Hz) for IGN, 7.0 (1.3Hz) for UCA and 7.0 (2.3Hz) for HCR. The average amplification factors are 4.9 for CIG, 7.3 for IGN, 4.6 for UCA and 7.0 for HCR. Here, the average amplification factor at HCR is equal to the maximum amplification factor because there is only a single peak on which the amplification occurs.

The E-W components *(Figure 12)*, indicate maximum spectral amplifications of 6.5 (2.8Hz) for CIG, 8.8 (2.1Hz) for IGN and 5.7 (3.0Hz) for HCR. Records from UCA are missing because of some instrumental problems. The average amplification factors for the same four sites are 4.0 for CIG, 6.3 for IGN and 3.5 for HCR.

Average of the two horizontal components indicate maximum amplifications in the order of 7.5 for CIG, 12.4 for IGN, 7.0 for UCA and 6.3 for HCR. The average amplification factors on the other hand are 4.5 for CIG, 6.8 for IGN, 4.6 for UCA and 3.5 for HCR.

STRONG MOTION:

The strong motion records are taken from the October 10, 1986 earthquake, which occurred close to the metropolitan area of San Salvador. The spectral amplification of the four sedimentary sites are calculated with respect to the reference site SHE situated on the eastern flank of the San Salvador Volcano. On previous studies the spectral amplifications of the five sedimentary sites were analyzed *(Atakan and Torres, 1993; Atakan and Figueroa, 1993).* For

this study we have only used the results for four of these sites. The interpretations related to these will not be repeated here.

For the N-S components the maximum amplification factors reach 15.0 for CIG, 22.0 for IGN, 7.8 for UCA and 17.0 for HCR, whereas the average values indicate 4.1 for CIG, 6.1 for IGN, 3.3 for UCA and 5.2 for HCR *(Figure 13)*. The E-W components gave somehow lower values *(Figure 14)*. The maximum amplifications for the E-W components are 6.0 for CIG, 6.5 for IGN, 4.6 for UCA and 4.6 for HCR. The average values are, 3.1 for CIG, 2.9 for IGN, 3.4 for UCA and 1.4 for HCR.

The average of the the two horizontal components indicate maximum amplifications in the order of 10.5 for CIG, 14.3 for IGN, 6.2 for UCA and 10.8 for HCR, whereas the average values are, 3.6 for CIG, 4.5 for IGN, 3.4 for UCA and 3.3 for HCR.

DISCUSSION:

Comparison was made based on the spectral ratios of four different data sets from the four sedimentary sites CIG, IGN, UCA and HCR. These are the microtremors, pre-event noise records, weak motion from the subduction zone earthquakes and strong motion from the Oct.10, 1986 earthquake. In order to provide a basis for these comparisons, some 3-D diagrams are prepared for N-S and E-W components showing the differences in maximum and average amplification factors between the four sedimentary sites, and are presented in *Figures 15 and 16*, respectively.

On the N-S components the average amplifications give systematically higher estimates at all sites for the pre-event noise records and the microtremors. Weak motion records give slightly lower estimates, but still higher than the strong motion records *(Figure 15)*. The only exception here is at HCR, however it should be noted that the average value is from a single peak and therefore is misleading. Regarding the comparison between the maximum and the average (being the average of amplifications at all individual peaks within the frequency range where spectral amplifications occur) spectral amplifications, the maximum amplifications do not show any good correlation between the different data sets and there is no preferred trend. The average amplification factors on the other hand, give more stable estimates and are not effected by the individual fluctuations at specific frequencies *(Figures*

15 and 16). This becomes especially clear when the average of the two horizontal components are considered *(Figure 17)*. This observation is probably related to the complexity of the lateral and vertical distribution of the sedimentary layers that cause the spectral amplifications with several peaks at different frequencies. The situation in San Salvador, therefore differs from the well known example of the case of Mexico City, where the site amplifications are related to a predominant frequency and give much higher factors *(Singh et al.,1988)*.

The spectral amplifications observed on strong motion records may be biased by the short source-receiver distances, especially when two of the stations, IGN and CIG lie along the direction where fault rupture propagated. This issue together with the problems related to the radiation pattern were discussed in an earlier study by Atakan and Torres *(1993)*. Although, these results may include some effects of the fault directivity, radiation pattern etc., the amplifications related to the local sediments seem to be predominant and overshadow the other possible influences. This is based on the observation that similar spectral amplifications in terms of the frequency ranges involved are observed also on the weak motion records from the subduction zone, where the assumptions related to the spectral ratio method are considered valid (i.e. far-field conditions where source to receiver distances are large enough to provide similar source and radiation pattern effects at all sites). In order to account for the possible radiation pattern and fault directivity effects, composite amplification factors, taking the average of four sites were calculated. These composite values for the maximum and the average amplification factors are shown in *Figure 18*. As expected, the largest standard deviation is observed on the maximum amplification factors from the strong motion records, where the effects are presumably highest. The standard deviation for the weak motion gives the lowest and hence the most stable in terms of the assumptions involved in spectral ratio analysis. However, the composite values for the average amplification factors seem to be quite stable with the lowest standard deviations for the strong motion data. The average amplification factors seem to smooth out these effects and are therefore more reliable than the maximum values in estimating the site response.

Regarding the background noise measurements, data were collected individually from each site with one-minute duration signals. Six such windows were recorded at each site and the best window in terms of the data quality was chosen for the analysis. Because of the limitations in the number of instruments used, no simultaneous measurements were taken between the different sites. This naturally introduces some uncertainty into microtremor data

set. In this sense, the pre-event noise records constitute a better data set, as they were collected at the sedimentary and the bedrock reference sites simultaneously. The results gave higher estimates from the pre-event noise records as compared to the microtremor measurements. However, the estimates were higher than the weak and strong motion in both cases. These assumptions and the uncertainties related to the background noise records therefore, have to be taken into consideration while interpreting the results.

CONCLUSIONS AND RECOMMENDATIONS:

The results of this study only demonstrate the importance of local site amplifications and compare different data sets that can be used in estimating these. It is obvious that, to improve our understanding of the behavior of the sedimentary layers to earthquake waves (i.e. the correlation between the observed spectral amplifications and the local geological conditions), more detailed studies on the geological and geotechnical characteristics of these sites are needed. The conclusions and the recommendations related to the spectral ratios given here, should therefore be treated carefully, bearing in mind the assumptions involved. Nevertheless, it is considered important that these are used as guide lines in any seismic hazard estimate, as they provide a clear indication of site amplifications and a rough estimate in the levels for the San Salvador metropolitan area. Here, following conclusions are deduced.

1. All four data sets, microtremors, pre-event noise records, weak ground motion and strong ground motion records, give spectral amplifications related to the local site conditions. The frequency range on which the amplifications observed vary at different data sets, however, a common frequency band of 1.0 to 10.0 Hz can be considered, assuming that this covers the frequency range of interest in terms of fundemental period of resonance in different building types (roughly from 1-storey to 10-storey buildings).

2. Within the frequency range of concern, the maximum amplifications vary from site to site and also between the different data sets. No preferred trend is observed among these. The average amplification factors, on the other hand, provide a more stable estimate of the spectral amplifications and a preferred trend of decreasing spectral amplification factors is observed starting from the pre-event noise records, to microtremors, weak motion and strong

motion. This is observed systematically on all four sites and therefore seems to be an indication of nonlinearity in the spectral amplifications, which is considered important.

3. Regarding the comparison between the data sets, the most realistic estimates are undoubtedly obtained from the strong motion records, as they represent the real target events. As to the strong motion record used in this study, there are a few considerations related to the radiation pattern, fault directivity etc., which may pose problems in the results obtained. However, as discussed earlier, the effect of these are considered to be overshadowed by the spectral amplifications related to the sedimentary layers. The maximum amplifications that can be expected from a local shallow source, similar to the October 10, 1986 earthquake, are in the range of 10 ± 6. On the average, spectral amplification of at least 4 ± 1 must be taken into account in any seismic hazard analysis in the metropolitan area of San Salvador, El Salvador.

4. The weak motion data set gives higher estimates than the strong motion data, however, they represent a better data set in terms of the assumptions involved in spectral ratio method. When calibrated with strong motion data, the estimates from the weak motion records can be regarded reliable. The average of the differences in spectral amplification factors at all four sites between the weak and the strong motion data, indicate values 1.6 ($\pm$ 0.89) higher on the weak motion records.

5. Relatively, the poorest estimates are obtained from the background noise measurements. Among the comparison between the random microtremor records and the pre-event noise records, the latter constitute a better data set in terms of the spectral ratios (i.e. the measurements were taken simultaneously both at the sedimentary and the bedrock reference site). However, both data sets overestimate the amplification factors. Unless calibrated with weak or strong motion, these records can only be used as a relative indication of spectral amplifications at different sites. The average of the differences between the microtremors and the strong motion records at all sites, indicate 1.9 ($\pm$ 0.91) higher on the microtremors. The differences for the pre-event noise records is 4.4 ($\pm$ 2.12) higher than the strong motion data.

Increased knowledge about the geological and geotechnical characteristics of the selected sites used in this study will naturally provide a better foundation for correlating with the spectral amplifications. In this respect, detailed studies of sediment lithology, lateral and vertical distribution of the different units etc., are needed. The ongoing efforts on this, can

be enlarged to include some specific investigations, such as simultaneous downhole and surface recordings of microtremors and/or earthquakes on the sites where boreholes were already drilled (IGN and UCA). They will provide a good calibration on the results obtained in this study.

The microtremor data obtained in this study can be extended to a more dense coverage of the metropolitan area of San Salvador (a study including 39 sites have already been initiated). Results from this, can be used to prepare a contour map of spectral amplification factors. Although, these would need a better calibration in terms of the absolute amplification factors, the relative distribution can still be used to understand the changes in spectral amplifications due to changes in the local geological conditions. Finally, similar studies from other major urban areas in El Salvador are needed, in order to have a more complete knowledge of the local site amplifications on population centers vulnareable to earthquake damage.

ACKNOWLEDGEMENTS:

We thank Centro de Investigaciones Geotécnicas, El Salvador, for providing the digitized accelerograph recordings and the logistic support during the field work. The geotechnical and the geological information is largely based on the unpublished work by the staff at the Dept. of Geology, Centro de Investigaciones Geotécnicas, El Salvador. Jane K. Ellingsen has kindly helped with the drawings. The computer program, used in calculating the spectral ratios (DEGTRA), is kindly provided by Mario Ordaz.

REFERENCES:

Aki,K. (1988). Local site effects on strong ground motion. Proc. Earthq. Eng. Soil Dyn. II. 103-155.

Aki,K. (1993). Local site effects on weak and strong ground motion. **IN:** F.Lund (Ed.), *New Horizons in Strong Motion: Seismic Studies and Engineering Practice.* Tectonophysics, **218**, 93-111.

Alvarez,S. (1987). Informe técnico-sismológico del terremoto de San Salvador del 10 de Octubre de 1986. (Internal Report) Ministerio de Obras Públicas, Centro de Investigaciones Geotécnicas, Departamento de Sismología, San Salvador, April 1987, 83p.

Atakan,K. and Figueroa,J.C. (1993). Local site response in San Salvador: Comparison between the synthetics and the observed ground motion of the October 10, 1986 earthquake. Report No.**8** under the project *"Reduction of Natural Disasters in Central America: Earthquake Preparedness and Hazard Mitigation"*, Institute of Solid Earth Physics, University of Bergen, Norway, 52p.

Atakan,K. and Torres,R. (1993). Local site response in San Salvador based on the earthquake of October 10, 1986. Report No.**6** under the project *"Reduction of Natural Disasters in Central America: Earthquake Preparedness and Hazard Mitigation"*, Institute of Solid Earth Physics, University of Bergen, Norway, 35p.

Boore,D.M., Seekins,L. and Joyner,W.B. (1989). Peak acceleration from the 17 October 1989 Loma Prieta earthquake. Seism. Res. Lett., **60**, 151-166.

Borcherdt,R.D. (1970). Effects of local geology on ground motion near San fransisco Bay. Bull. Seism. Soc. Am. **60**, 29-61.

Borcherdt,R.D., and Gibbs,J.F. (1976). Effects of local geological conditions in the region on ground motions and the intensities of the 1906 earthquakes. Bull. Seism. Soc. Am. **66**, 467-500.

Borcherdt,R.D., Glassmoyer,G., Der Kiureghian,A., and Cranswick,E. (1989). Results and data from seismologic and geologic studies following earthquakes of December 7, 1988 near Spitak, Armenia, S.S.R., U.S.Geol.Surv. Open-File Report, 89-163A.

Burke,K., Cooper,C., Dewey,J.F., Mann,P. and Pindell,J.I. (1984). Carribean Tectonics and relative plate motions, in Caribbean-South-American plate. Mem. Geol. Soc. Am., **162**, 31-63.

Centro de Investigaciones Geotécnicas (1987). Mapa geológico-tectónico del área San Salvador y alrededores. Esc: 1:15 000.

Dengo,G. (1985). Mid-America: Tectonic setting for the Pacific margin from southern Mexico to northwestern Colombia. **IN:** H.E.M.Naim, F.G.Stehli, and S.Uyeda (Eds.), *The Ocean Basins and Margins.* Plenum, New York, 123-180.

Durr,F., et al. (1960). Energía Geotérmica. Informe No.1, Servicio Geológico Nacional, San Salvador, 268p.

Field,E.H., Jacob,K.H., and Hough,S.E. (1992). Earthquake site response estimation: a weak motion case study. Bull. Seism. Soc. Am., **82**, 2283-2307.

Harlow,D.H., White,R.A., Rymer,M.J. and Alvarez,G.S. (1993). The San Salvador earthquake of 10 October 1986 and its historical context. Bull. Seismol. Soc. Am., Vol.**83**, No.4, 1143-1154.

Hartzell,S.H. (1992). Site response estimation from earthquake data. Bull. Seism. Soc. Am., **82**, 2303-2327.

Herrmann,R.B. (1985). Computer programs in Earthquake Seismology. Vol.**VI**: Regional Seismograms: Wavenumber Integration. Saint Louis University, Missouri, U.S.A.

Hough,S.E., Borcherdt,R.D., Friberg,P.A., Busby,R., Field,E., and Jacob,K.H. (1990). the role of sediment-induced amplification in the collapse of the Nimitz freeway during the October 17, 1989 Loma Prieta earthquake. Nature **344**, 853-855.

Italtekna/Italconsult (1987). Studi di risposta sismica locale ed elaborazione delle carte di microzonazione sismica. (Unpbl. Report) Consorzio Salvador e San Salvador Programma di Ricostruzione, Republica Italiana, Ministerio Degli Affari Esteri Direzione generale Per La Cooperazione Allo Sviluppo, Parte 4a, 67p.

Lermo,J.F. and Chávez-García,F.J. (1993). Site effect evaluation using spectral ratios with only one station. Bull. Seismol. Soc. Am., Vol.**83**, N0.5., 1574-1594.

Lermo,J., Rodriguez,M., and Singh,S.K. (1988). The Mexico earthquake of September 19, 1985: natural period of sites in the valley of Mexico from microtremor measurements and from strong motion data. Earthquake Spectra **4**, 805-814.

Malfait,B.T., and Dinkelmann,M.G. (1972). Circum-Caribbean tectonic and Igneous activity and the evolution of the Caribbean plate. Geol. Soc. Am. Bull., **83**, 251-271.

Mann,P., and Burke,K. (1984). Neotectonics of the Caribbean, Rev. Geophys., **22**, 309-362.

Milne,J. (1898). Seismology. 1st ed., London, Kegan Paul, Trench, Truber.

Molnar,P., and Sykes,L.R. (1969). Tectonics of the Caribbean and the Middle America regions from focal mechanisms and seismicity. Geol. Soc. Am. Bull., **89**, 1639-1684.

Nakamura,Y. (1989). A method for dynamic characteristics estimation of subsurface using microtremor on the ground surface, QR o RTR1 **30**, 1, February.

Olson,R.A. (1987). The San Salvador earthquake of October 10, 1986: overview and context. Earthquake spectra, Vol.**3**, No.3, 415-435.

Rogers,A.M., Borcherdt,R.D., Covington,P.A., and Perkins,D.M. (1984). A comparative ground response study near Los Angeles using recordings of Nevada nuclear tests and the 1971 San Fernando earthquake. Bull. Seism. Soc. Am. **74**, 1925-1949.

Rymer,M.J. (1987). The San Salvador earthquake of October 10, 1986 - Geological aspects. Earthquake Spectra, Vol.**3**, No.3, 436-462.

Shakal,A.F., Huang,M.J., Parke,D.L., and Linares,R. (1986). Summary of the processed strong-motion data, San Salvador earthquake of October 10, 1986. Proceedings from the San Salvador Earthquake Briefing, Nov.24, 1986, Washington D.C., U.S.A.

Singh, S.K., Lermo,J., Dominguez,T., Ordaz,M., Espinoza,J.M., Mena,E., and Quass,R. (1988). the Mexico earthquake of September 19, 1985: a study of amplification of seismic waves in the Valley of Mexico with respect to a hill zone site. Earthquake Spectra **4**, 653-673.

Schmidt-Thomé,M. (1975). The geology in the San Salvador area (El Salvador, Central America), a basis for city development and planning. Geologisches Jahrbuch, v.**13**, 207-228.

Şafak,E. (1991). Problems with using spectral ratios to estimate site amplification. Proc.Forth Int. Conf. on Seismic Zonation, Stanford, California, **II**, 277-284.

Weber, H.S., Weisemann,G., Lorenz,H., and Schmidt-Thomé,M. (1978). Mapa geológico de la República de El Salvador / América Central: Bundesanstalt für Geowissenschaften und Roshtoffe, Hannover, Germany, Scale: 1:100 000.

Weinberg,R.F. (1992). Neotectonic development of Western Nicaragua. Tectonics, Vol.**11**, No.5, 1010-1017.

Weisemann, G. (1975). Remarks on the geologic structure of the Republic of El Salvador, Central America: Mitteilungen Geologisch-Palaontologischen Institut, University of Hamburg, v.**44**, 557-574.

White,R.A., Harlow,D.H. and Alvarez,S. (1987). The San Salvador earthquake of October 10, 1986 - Seismological aspects and other recent local seismicity. Earthquake Spectra, Vol.**3**, No.3, 419-434.

White,R.A. and Harlow,D.H. (1993). Destructive upper crustal earthquakes of Central America since 1900. Bull. Seismol. Soc. Am., Vol.**83**, No.4, 1115-1142.

FIGURE CAPTIONS:

Figure 1. The locations of the five accelerograph stations used in this study. At each site, the N-S component of the acceleration recordings from the October 10, 1986 earthquake are shown for comparison. Note the lower amplitudes at SHE. The major roads are shown for orientation.

Figure 2.a. Map showing the geology of the San Salvador area *(Simplified from the 1:15 000 geological map prepared by Centro de Investigaciones Geotécnicas, 1987).* Major fault trends,

as well as the main roads are shown. **b.** The parallel N-S cross-sections, AA' AND BB', showing the lithology and thickness variations. The numbers at each site indicates the results from the penetrations tests.

Figure 3. The mainshock and the immediate aftershocks (within the first 24 hours) of the October 10, 1986 earthquake *(from Harlow et al., 1993)*. The first intermadiate aftershock (M_S=4.8) is shown on the northern part of the city. The cross-section AA' clearly shows the steeply dipping fault plane. Modified Mercalli intensity contours VII and VIII are also shown.

Figure 4. Damaging upper crustal earthquakes in the San Salvador area from 1700 to 1990. Modified Mercalli intensity contour VII is shown for each event *(from White and Harlow, 1993)*.

Figure 5. The macroseismic intensity (Modified Mercalli) contour map *(from Alvarez, 1987)*. The distribution of damage is also shown with darker patterns indicating higher damage *(modified from Centro de Investigaciones Geotécnicas, 1987)*. The stars indicate the areas where total damage to buildings occurred. the epicenter of the October 10, 1986 earthquake is also shown by a larger star. Stippled line indicates the city limits. Note that the distribution is largely along a NNE-SSW trend.

Figure 6. Epicenter distribution of the earthquakes from the subduction zone, used in the weak motion data set. Among the 16 events shown, only 9 of them were used in the analysis *(see Table II)*.

Figure 7. The spectral plots and the spectral ratios (right hand side) of N-S components of the microtremor records from four sedimentary sites with respect to the bedrock reference site SJA. The solid lines are the spectra corresponding to the sedimentary sites, whereas the dashed lines indicate the spectra of the bedrock reference site.

Figure 8. The spectral plots and the spectral ratios (right hand side) of E-W components of the microtremor records from three sedimentary sites with respect to the bedrock reference site SHE. The solid lines are the spectra corresponding to the sedimentary sites, whereas the dashed lines indicate the spectra of the bedrock reference site. Data from IGN is missing due to instrumental problems.

Figure 9. The spectral plots and the spectral ratios (right hand side) of N-S components of the pre-event noise records from four sedimentary sites with respect to the bedrock reference sites SJA and SOC. The solid lines are the spectra corresponding to the sedimentary sites, whereas the dashed lines indicate the spectra of the bedrock reference site.

Figure 10. The spectral plots and the spectral ratios (right hand side) of E-W components of the pre-event noise records from three sedimentary sites with respect to the bedrock reference sites SJA and SOC. The solid lines are the spectra corresponding to the sedimentary sites, whereas the dashed lines indicate the spectra of the bedrock reference site. Data from UCA is missing due to instrumental problems.

Figure 11. The spectral plots and the spectral ratios (right hand side) of N-S components of the weak motion records from four sedimentary sites with respect to the bedrock reference sites SJA and SOC. The solid lines are the spectra corresponding to the sedimentary sites, whereas the dashed lines indicate the spectra of the bedrock reference site.

Figure 12. The spectral plots and the spectral ratios (right hand side) of E-W components of the weak motion records from three sedimentary sites with respect to the bedrock reference sites SJA and SOC. The solid lines are the spectra corresponding to the sedimentary sites, whereas the dashed lines indicate the spectra of the bedrock reference site. Data from UCA is missing due to instrumental problems.

Figure 13. The spectral plots and the spectral ratios (right hand side) of N-S components of the strong motion records from four sedimentary sites with respect to the bedrock reference site SHE. The solid lines are the spectra corresponding to the sedimentary sites, whereas the dashed lines indicate the spectra of the bedrock reference site. Amplitudes are in cm/sec^2.

Figure 14. The spectral plots and the spectral ratios (right hand side) of E-W components of the strong motion records from four sedimentary sites with respect to the bedrock reference site SHE. The solid lines are the spectra corresponding to the sedimentary sites, whereas the dashed lines indicate the spectra of the bedrock reference site. Amplitudes are in cm/sec^2.

Figure 15. Average and maximum amplification factors for the N-S components of the four sedimentary sites. All four data sets are shown for comparison. "Noise (W)" represents the pre-event noise records whereas "Noise" represents the microtremors.

Figure 16. Average and maximum amplification factors for the E-W components of the four sedimentary sites. All four data sets are shown for comparison. "Noise (W)" represents the pre-event noise records whereas "Noise" represents the microtremors.

Figure 17. Average and maximum amplification factors for the average of the two horizontal components of the four sedimentary sites. All four data sets are shown for comparison. "Noise (W)" represents the pre-event noise records whereas "Noise" represents the microtremors.

Figure 18. Composite amplification factors for the average and the maximum values for the four data sets. Composite values are calculated by taking the arithmetic mean of the four sedimentary sites. The standart deviations are also shown.

Table I. Combinations of sites used for spectral ratio analyses. Data recording codes are also indicated.

Component	N - S				E - W			
Type of Signal	Noise (W)	Noise (R)	Weak motion	Strong motion	Noise (W)	Noise (R)	Weak motion	Strong motion
CIG	CIG/ SJA e01	CIG/ SJA n5/n9	CIG/ SJA e01	CIG/ SHE f05/f23	CIG/ SJA e01	CIG/ SHE n5/n6	CIG/ SJA e01	CIG/ SHE f05/f23
IGN	IGN/ SJA e04	IGN/ SJA n4/n9	IGN/ SJA e04	IGN/ SHE f02/f23	IGN/ SOC e14	bad record	IGN/ SOC e14	IGN/ SHE f02/f23
UCA	UCA/ SJA e03	UCA/ SJA n5/n9	UCA/ SJA e03	UCA/ SHE f20/f23	bad record	UCA/ SHE n5/n6	bad record	UCA/ SHE f20/f23
HCR	HCR/ SOC e15	HCR/ SJA n3/n9	HCR/ SOC e15	HCR/ SHE f11/f23	HCR/ SOC e15	HCR/ SHE n3/n6	HCR/ SOC e15	HCR/ SHE f11/f23

Table II. List of earthquakes from the subduction zone, used in the weak motion data set.

No.	Year	Date mm dd	Time hh:mm	Lat. (N)	Lon. (W)	Depth (km)	No. Stat	rms (sec)	M_C
1*	1992	10 25	09:54	13.077	89.078	50.0	17	0.1	4.1
2	1992	10 28	23:09	12.874	89.017	23.6	18	0.1	3.9
3*	1992	10 29	06:40	12.660	88.886	11.0	14	0.1	4.1
4*	1992	11 05	08:52	13.001	89.190	37.0	18	0.2	3.8
5	1992	12 05	09:52	13.134	89.601	31.6	18	0.1	4.0
6*	1992	12 09	19:28	13.224	88.804	72.2	18	0.1	4.6
7*	1993	04 27	05:56	12.893	88.445	46.8	16	0.2	4.2
8	1993	04 28	09:16	12.499	88.125	35.2	15	0.2	4.8
9*	1993	04 30	10:01	13.184	89.218	51.6	16	0.1	4.3
10	1993	04 30	12:29	14.104	92.426	50.0	16	0.3	5.3
11	1993	05 03	17:14	12.850	88.872	50.0	17	0.3	4.5
12	1993	05 22	04:51	13.940	90.740	50.0	12	0.3	5.1
13	1993	05 22	22:55	12.954	89.042	17.8	15	0.1	4.7
14*	1993	07 01	05:55	12.649	88.498	50.0	15	0.4	4.4
15*	1993	07 22	18:31	13.163	89.607	35.2	18	0.2	4.6
16*	1993	07 30	10:11	13.498	90.950	34.7	16	0.3	4.2

* *Events used in the spectral ratio analysis.*

Table III. Average spectral amplification factors at four sedimentary sites. Averages are calculated by taking the mean value of amplifications at individual peaks within the frequency range (shown by small numbers in Hz under each value), on which the amplifications observed. "Noise (W)", indicates the pre-event noise records, whereas "Noise (R)" is for microtremors.

Component	N - S				E - W			
Type of Signal	Noise (W)	Noise (R)	Weak motion	Strong motion	Noise (W)	Noise (R)	Weak motion	Strong motion
CIG	10.4 0.9 - 10.0	6.37 1.0 - 10.0	4.93 0.7 - 10.0	4.1** 0.4 - 4.0	7.76 1.0 -10.0	4.55** 1.0 - 10.0	4.03 1.0 -10.0	3.1** 1.0 -10.0
IGN	11.1 1.0 -10.0	8.54 1.0 - 10.0	7.32 0.7 - 9.0	6.1** 0.4 - 4.0	10.07* 1.2 - 10.0	bad record	6.28* 0.5 - 10.0	2.9** 0.4 - 4.0
UCA	6.0 2.0 - 10.0	6.35 1.0 - 10.0	4.56 0.5 - 6.0	3.3** 0.4 - 6.0	bad record	3.89** 1.0 - 10.0	bad record	3.4** 0.4 - 7.0
HCR	5.51* 2.0 - 5.0	6.0 1.0 -10.0	=max.amp	5.2** 0.4 - 6.0	6.21* 1.0 - 10.0	4.09** 1.0 - 10.0	3.5* 1.0 - 5.0	1.4** 0.4 - 5.0

* Corrected for SOC/SJA

** Corrected for SHE/SJA

Table IV. Maximum spectral amplification factors at four sedimentary sites. Maximum values are amplifications at individual peaks with specific frequencies, shown in Hz, in paranthesis. "Noise (W)", indicates the pre-event noise records, whereas "Noise (R)" is for microtremors.

Component	N - S				E - W			
Type of Signal	Noise (W)	Noise (R)	Weak motion	Strong motion	Noise (W)	Noise (R)	Weak motion	Strong motion
CIG	27.0 (4.9)	10.5 (3.0)	8.5 (2.1)	15.0** (1.3)	11.0 (4.0)	9.0** (8.4)	6.5 (2.8)	6.0** (3.5)
IGN	20.0 (2.4)	17.0 (2.0)	16.0 (2.9)	22.0** (0.7)	14.06* (7.0)	bad record	8.78* (2.1)	6.5** (1.3)
UCA	21.0 (3.5)	11.0 (2.4)	7.0 (1.3)	7.8** (1.2)	bad record	4.2** (3.5)	bad record	4.6** (2.3)
HCR	6.2* (2.4)	12.0 (2.5)	7.0* (2.3)	17.0** (0.7)	8.36* (10.0)	5.05** (7.2)	5.68* (3.0)	4.6** (0.4)

* Corrected for SOC/SJA

** Corrected for SHE/SJA

Table V. Average and maximum spectral amplification factors of the average of the two horizontal components of the four sedimentary sites. "Noise (W)" indicates the pre-event noise records, whereas "Noise (R)" indicate the microtremor records.

Amp.Fac.	**AVE.** (NS-EW)				**MAX.** (NS-EW)			
Type of Signal	Noise (W)	Noise (R)	Weak motion	Strong motion	Noise (W)	Noise (R)	Weak motion	Strong motion
CIG	9.08	5.46	4.48	3.60	19.00	9.75	7.50	10.50
IGN	10.59	8.54	6.80	4.50	17.03	17.00	12.39	14.25
UCA	6.00	5.12	4.56	3.35	21.00	7.60	7.00	6.20
HCR	5.86	5.05	3.50	3.30	7.28	8.53	6.34	10.80

Table VI. Composite (being the average of the four sedimentary sites) spectral amplification factors of the average and maximum values. Standard deviation for each are also shown. "Noise (W)" indicates the pre-event noise records, whereas "Noise (R)" indicate the microtremor records.

Composite Amp.Fac.	**AVE.** (NS-EW)				**MAX.** (NS-EW)			
Type of Signal	Noise (W)	Noise (R)	Weak motion	Strong motion	Noise (W)	Noise (R)	Weak motion	Strong motion
Mean	8.15	5.68	5.10	3.69	15.37	9.82	8.49	10.44
St.dev.	2.17	1.52	1.31	1.36	6.99	4.02	3.23	6.20

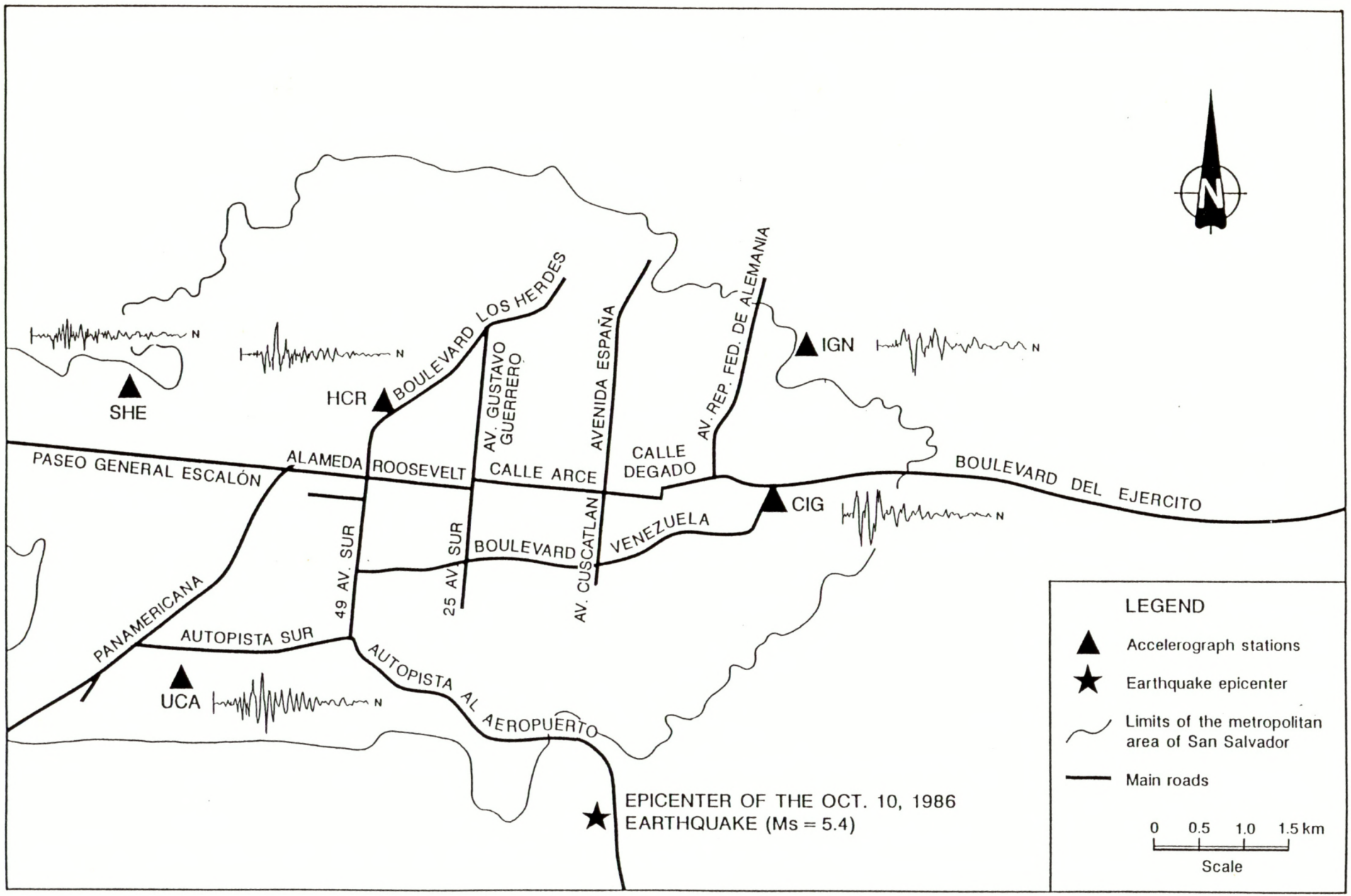
N
SHE
HCR
IGN
CIG
UCA
BOULEVARD LOS HEROES
AV. GUSTAVO GUERRERO
AVENIDA ESPAÑA
AV. REP. FED. DE ALEMANIA
PASEO GENERAL ESCALÓN
ALAMEDA ROOSEVELT
CALLE ARCE
CALLE DEGADO
BOULEVARD DEL EJERCITO
49 AV. SUR
25 AV. SUR
BOULEVARD VENEZUELA
AV. CUSCATLAN
PANAMERICANA
AUTOPISTA SUR
AUTOPISTA AL AEROPUERTO
EPICENTER OF THE OCT. 10, 1986 EARTHQUAKE (Ms = 5.4)
LEGEND
Accelerograph stations
Earthquake epicenter
Limits of the metropolitan area of San Salvador
Main roads
0 0.5 1.0 1.5 km
Scale

Figure 1.

B'
A'
A
B
N
0.0 0.5 1.0 1.5
Scale (km)
LEGEND
Alluvium (Recent)
Volcanic Ash (Holocene)
Tuffs (Pleistocene)
Volcanic Scoria (Pleistocene)
Basaltic and Andesitic Lava (Pleistocene)
Basaltic, Andesitic and Dacitic Lava (Pliocene - Pleistocene)
Basaltic and Andesitic Lava (Pliocene)
Formation Boundaries
Main Roads
Faults

Figure 2a.

Figure 2b.

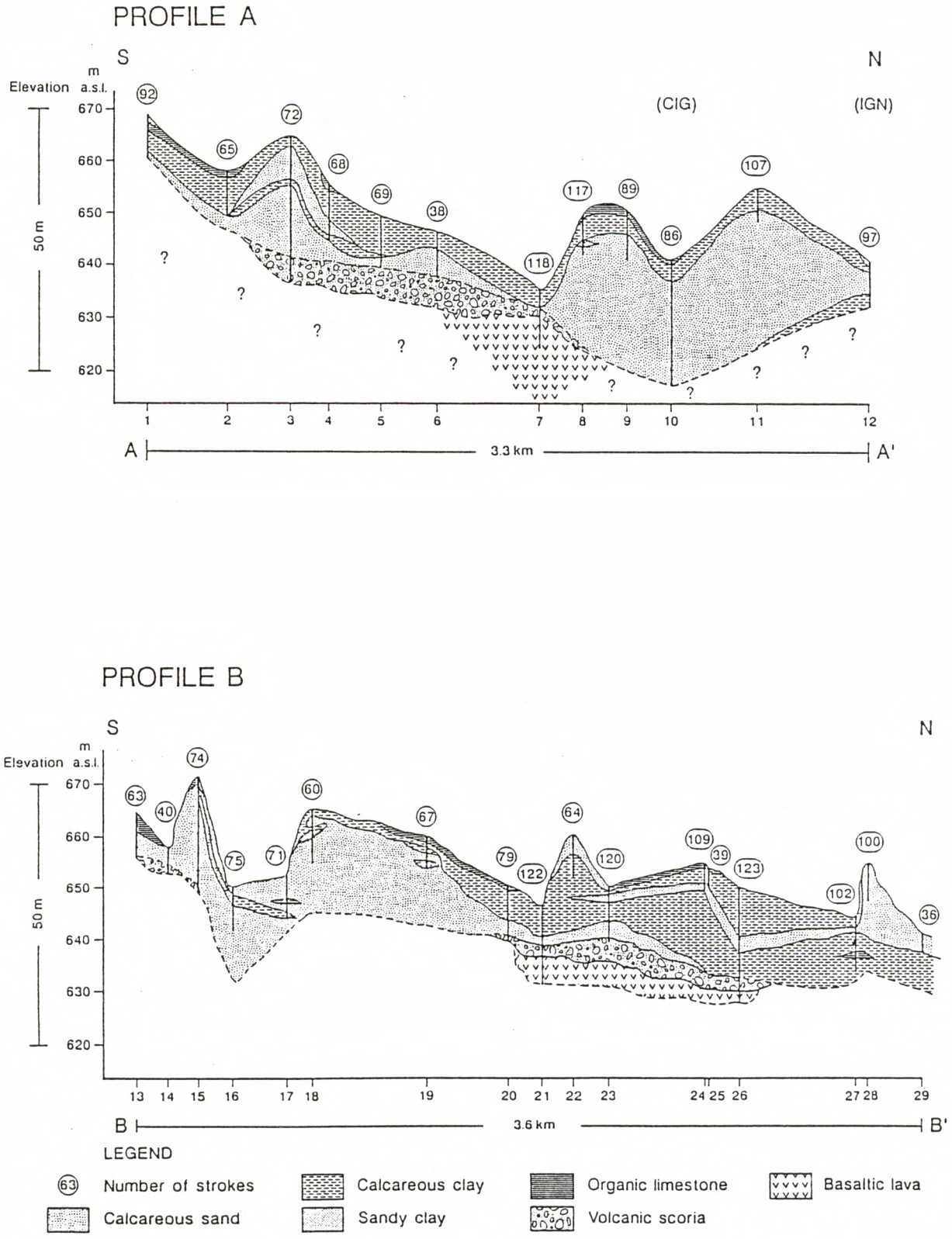
PROFILE A
S
N
m
Elevation a.s.l.
(CIG)
(IGN)
670
660
650
640
630
620
50 m
92
72
65
68
69
38
118
117
89
86
107
97
1
2
3
4
5
6
7
8
9
10
11
12
A
3.3 km
A'
PROFILE B
S
N
m
Elevation a.s.l.
74
63
40
60
67
64
75
71
79
122
120
109
39
123
100
102
36
13
14
15
16
17
18
19
20
21
22
23
24
25
26
27
28
29
B
3.6 km
B'
LEGEND
63 Number of strokes
Calcareous sand
Calcareous clay
Sandy clay
Organic limestone
Volcanic scoria
Basaltic lava

Figure 3.

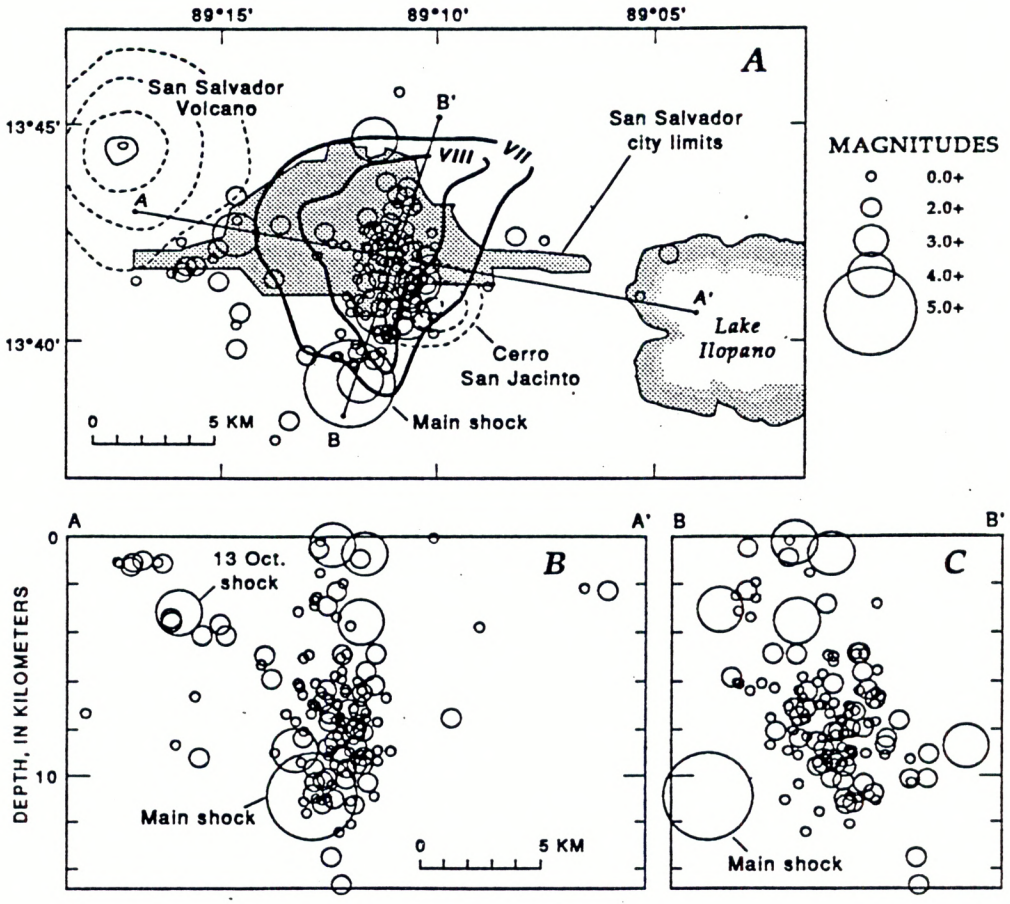
89°15'
89°10'
89°05'
A
13°45'
13°40'
San Salvador Volcano
B'
VIII
VII
San Salvador city limits
A
A'
Lake Ilopango
Cerro San Jacinto
0
5 KM
B
Main shock
MAGNITUDES
0.0+
2.0+
3.0+
4.0+
5.0+
A
A'
B
B'
0
10
DEPTH, IN KILOMETERS
13 Oct. shock
B
C
Main shock
0
5 KM
Main shock

Figure 4.

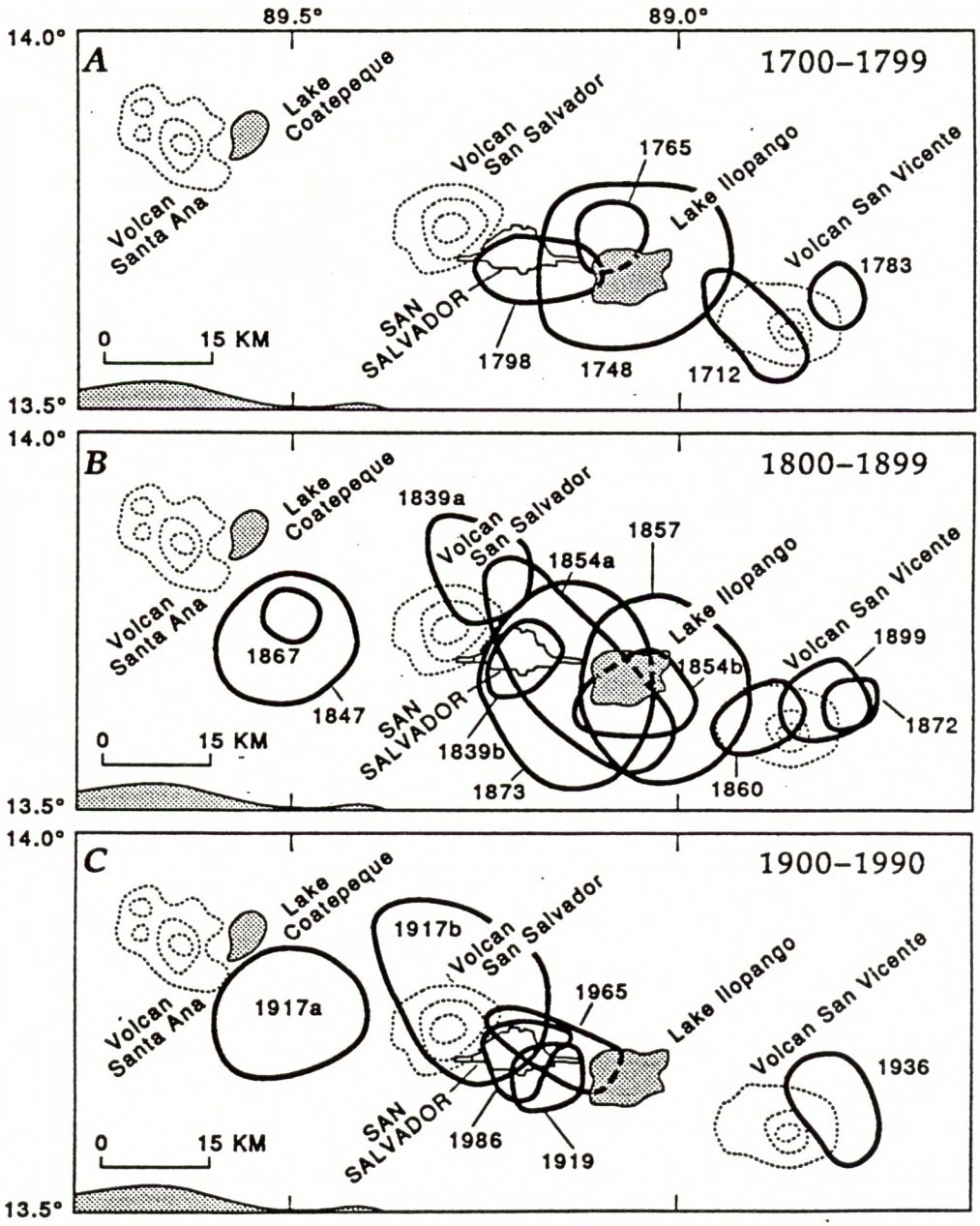
89.5°
89.0°
14.0°
13.5°
A
1700–1799
Lake Coatepeque
Volcan Santa Ana
Volcan San Salvador
1765
Lake Ilopango
Volcan San Vicente
1783
SAN SALVADOR
1798
1748
1712
0 15 KM
B
1800–1899
1839a
1857
1854a
1867
1847
1854b
1899
1872
1839b
1873
1860
C
1900–1990
1917b
1917a
1965
1936
1986
1919

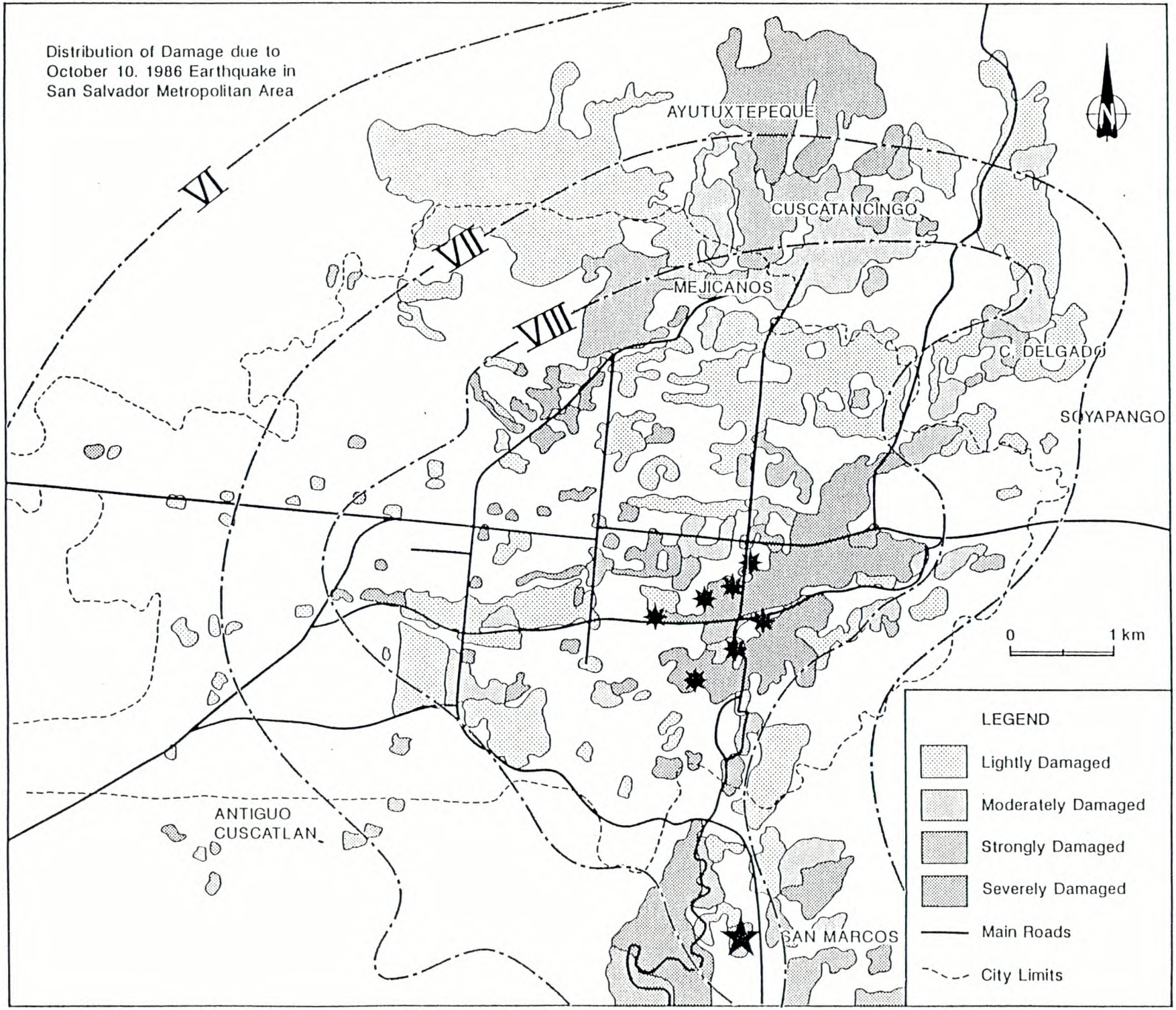
Distribution of Damage due to
October 10. 1986 Earthquake in
San Salvador Metropolitan Area
AYUTUXTEPEQUE
CUSCATANCINGO
MEJICANOS
C. DELGADO
SOYAPANGO
ANTIGUO
CUSCATLAN
SAN MARCOS
VI
VII
VIII
N
0
1 km
LEGEND
Lightly Damaged
Moderately Damaged
Strongly Damaged
Severely Damaged
Main Roads
City Limits

Figure 5.

Figure 6.

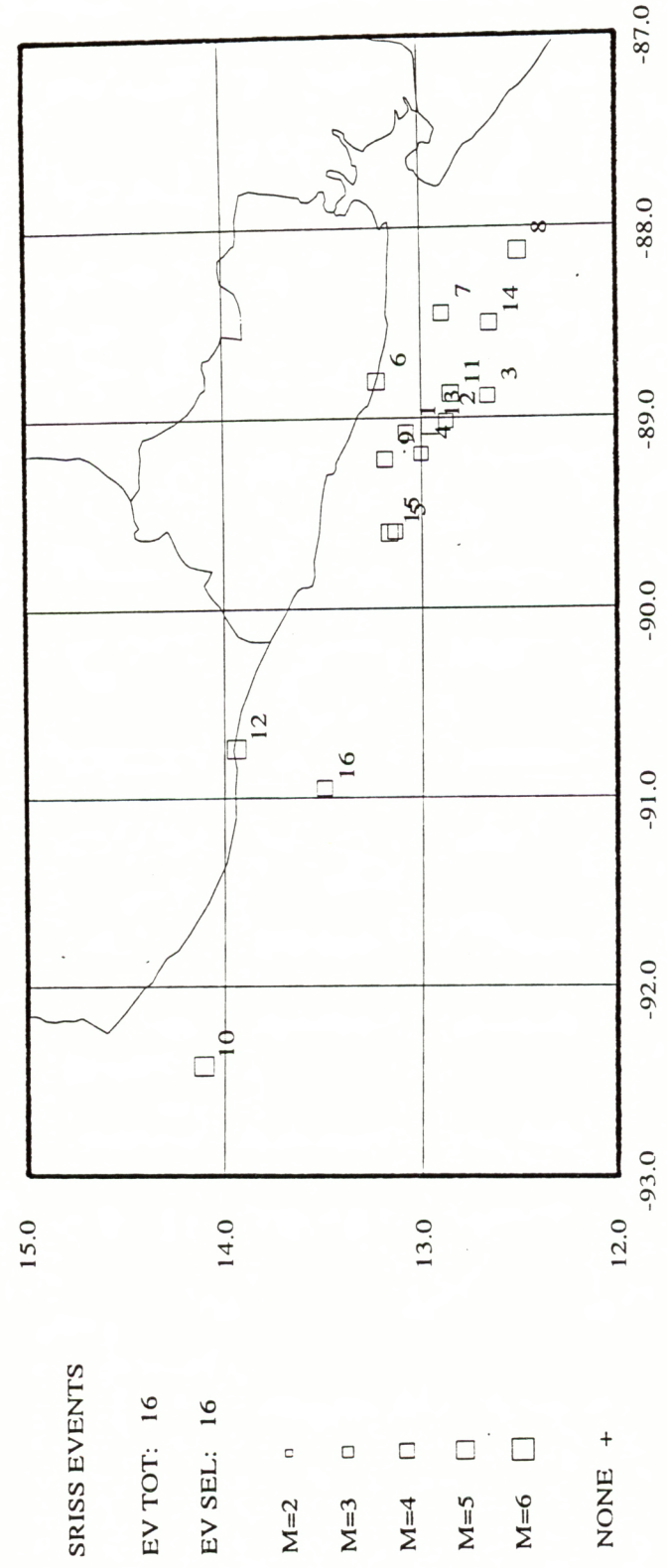
SRISS EVENTS
EV TOT: 16
EV SEL: 16
M=2
M=3
M=4
M=5
M=6
NONE +
15.0
14.0
13.0
12.0
-93.0
-92.0
-91.0
-90.0
-89.0
-88.0
-87.0

Figure 7.

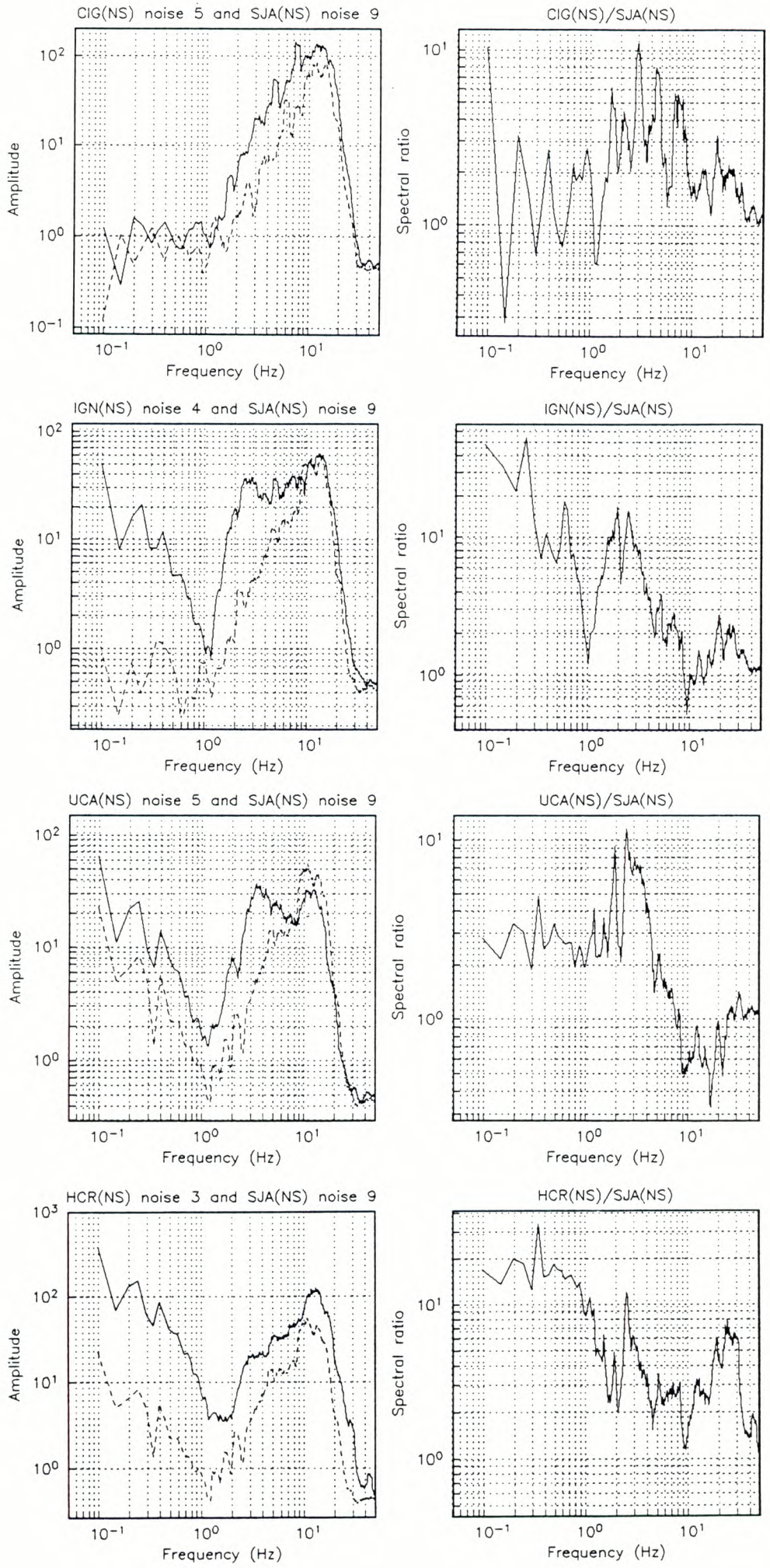
CIG(NS) noise 5 and SJA(NS) noise 9
CIG(NS)/SJA(NS)
IGN(NS) noise 4 and SJA(NS) noise 9
IGN(NS)/SJA(NS)
UCA(NS) noise 5 and SJA(NS) noise 9
UCA(NS)/SJA(NS)
HCR(NS) noise 3 and SJA(NS) noise 9
HCR(NS)/SJA(NS)
Amplitude
Spectral ratio
Frequency (Hz)

Figure 8.

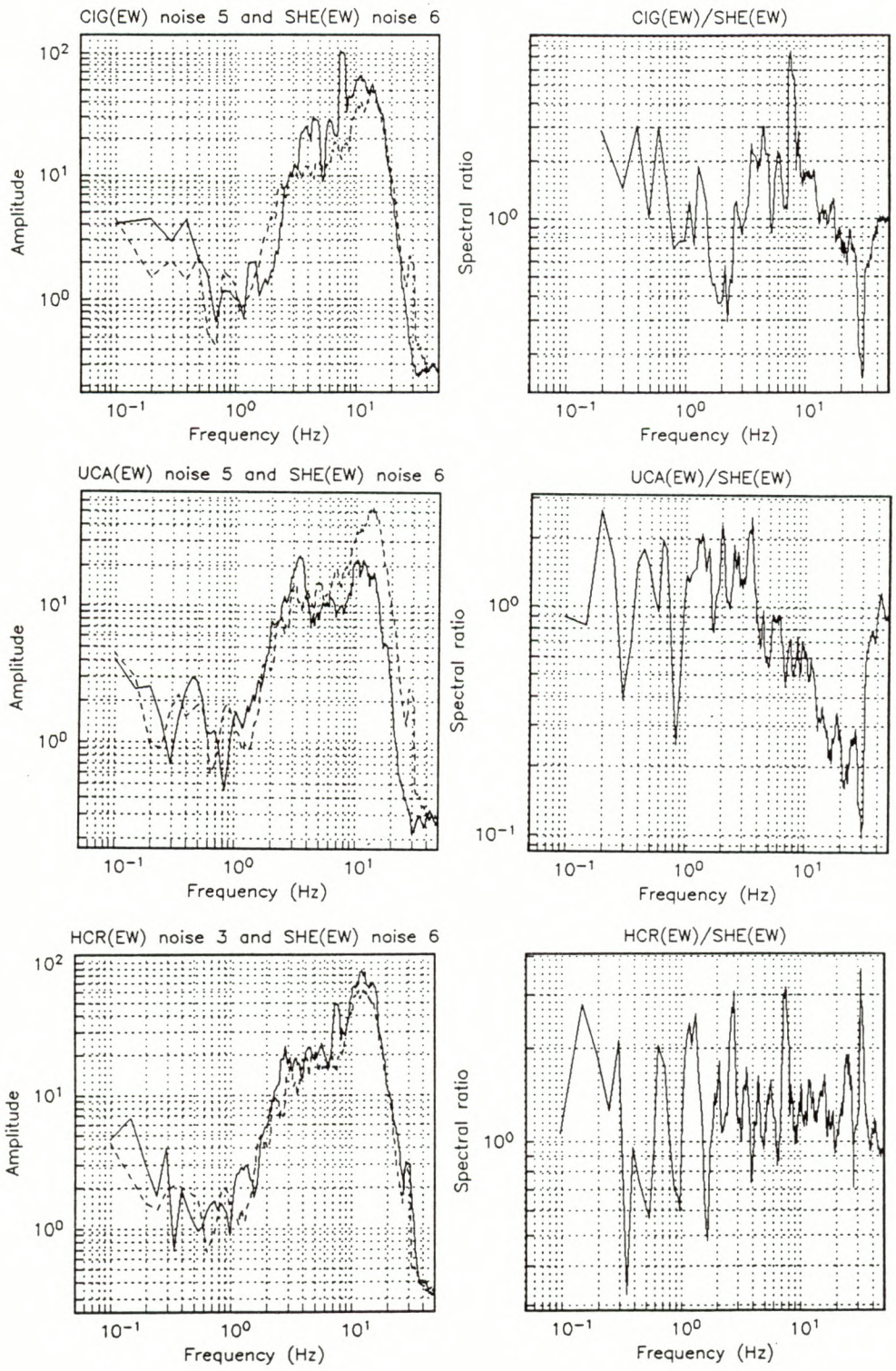
CIG(EW) noise 5 and SHE(EW) noise 6
CIG(EW)/SHE(EW)
UCA(EW) noise 5 and SHE(EW) noise 6
UCA(EW)/SHE(EW)
HCR(EW) noise 3 and SHE(EW) noise 6
HCR(EW)/SHE(EW)
Amplitude
Spectral ratio
Frequency (Hz)
10^{2}
10^{1}
10^{0}
10^{-1}

Figure 9.

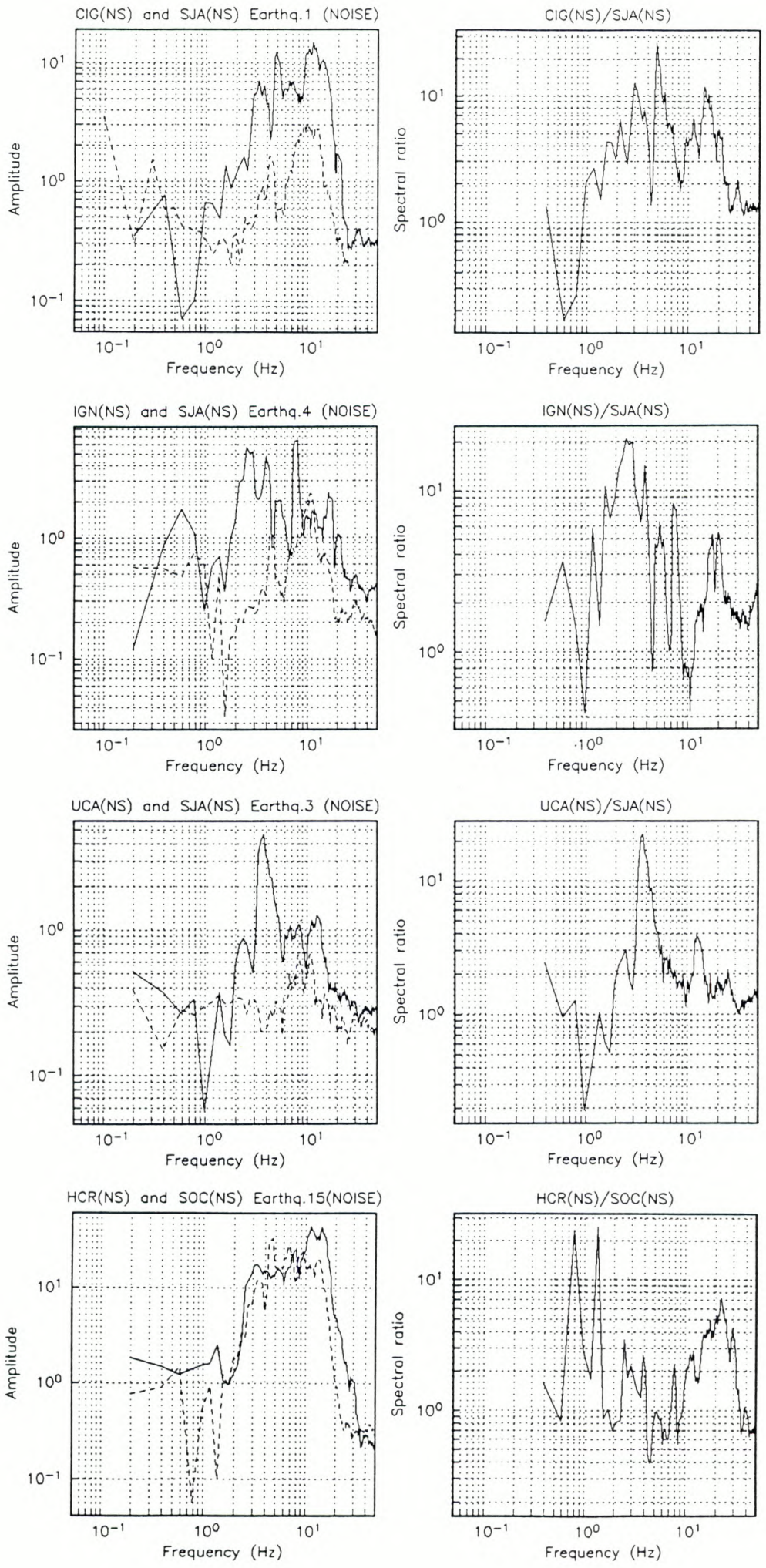
CIG(NS) and SJA(NS) Earthq.1 (NOISE)
CIG(NS)/SJA(NS)
IGN(NS) and SJA(NS) Earthq.4 (NOISE)
IGN(NS)/SJA(NS)
UCA(NS) and SJA(NS) Earthq.3 (NOISE)
UCA(NS)/SJA(NS)
HCR(NS) and SOC(NS) Earthq.15(NOISE)
HCR(NS)/SOC(NS)
Amplitude
Spectral ratio
Frequency (Hz)
10^{-1}
10^{0}
10^{1}

Figure 10.

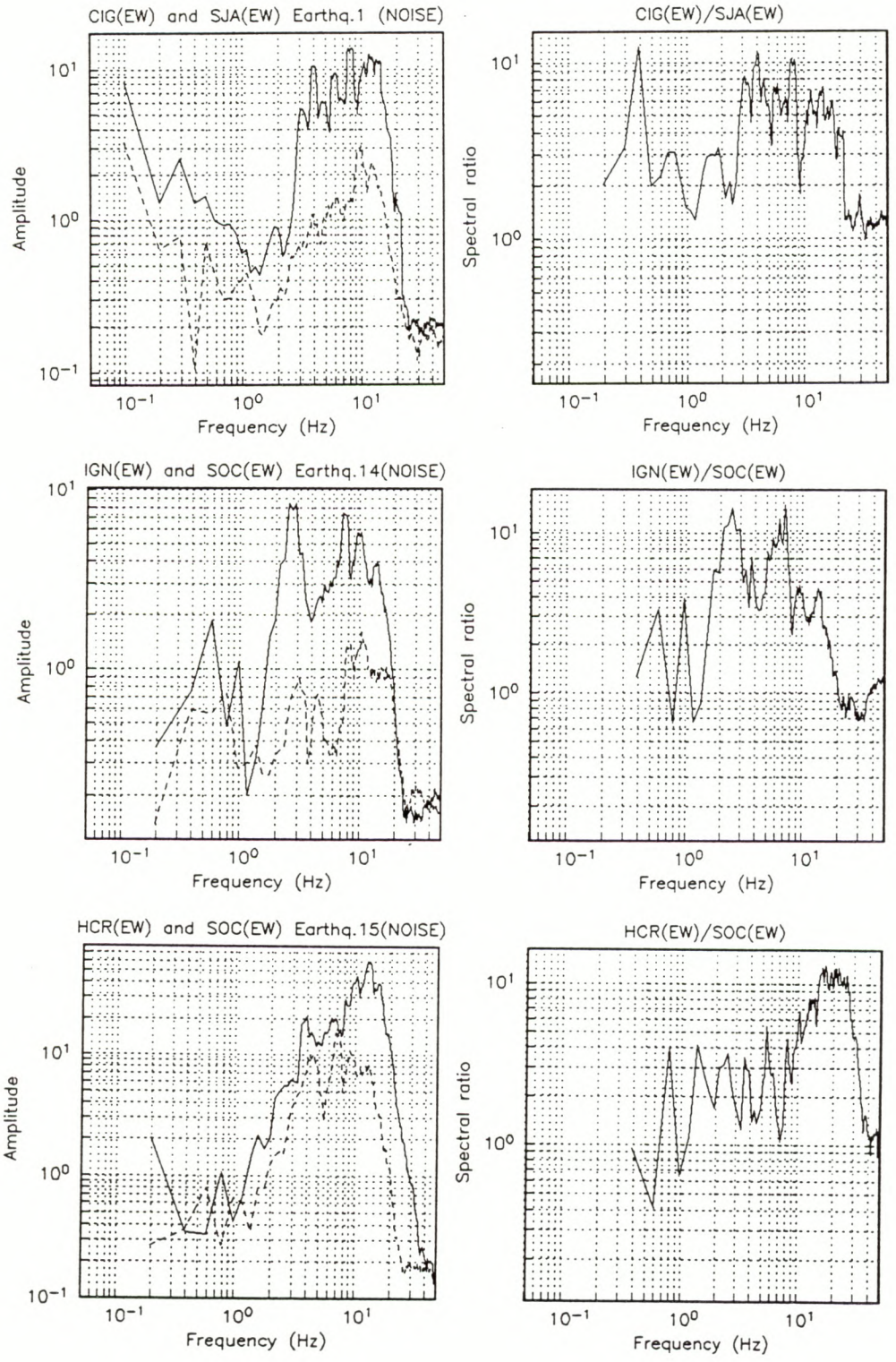
CIG(EW) and SJA(EW) Earthq.1 (NOISE)
CIG(EW)/SJA(EW)
IGN(EW) and SOC(EW) Earthq.14(NOISE)
IGN(EW)/SOC(EW)
HCR(EW) and SOC(EW) Earthq.15(NOISE)
HCR(EW)/SOC(EW)
Amplitude
Spectral ratio
Frequency (Hz)
10^{1}
10^{0}
10^{-1}

Figure 11.

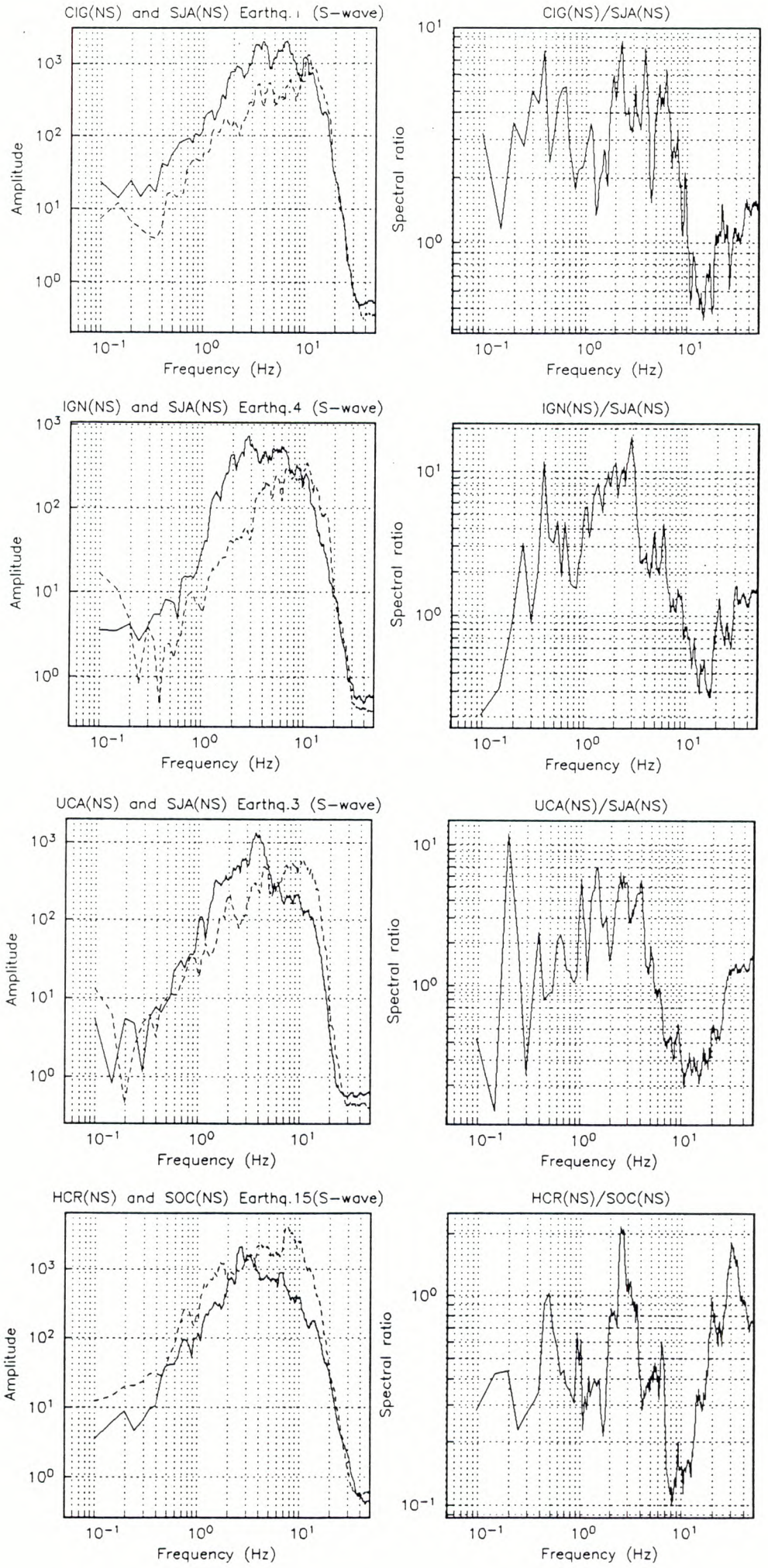
CIG(NS) and SJA(NS) Earthq. 1 (S-wave)
CIG(NS)/SJA(NS)
IGN(NS) and SJA(NS) Earthq.4 (S-wave)
IGN(NS)/SJA(NS)
UCA(NS) and SJA(NS) Earthq.3 (S-wave)
UCA(NS)/SJA(NS)
HCR(NS) and SOC(NS) Earthq.15(S-wave)
HCR(NS)/SOC(NS)
Amplitude
Spectral ratio
Frequency (Hz)

Figure 12.

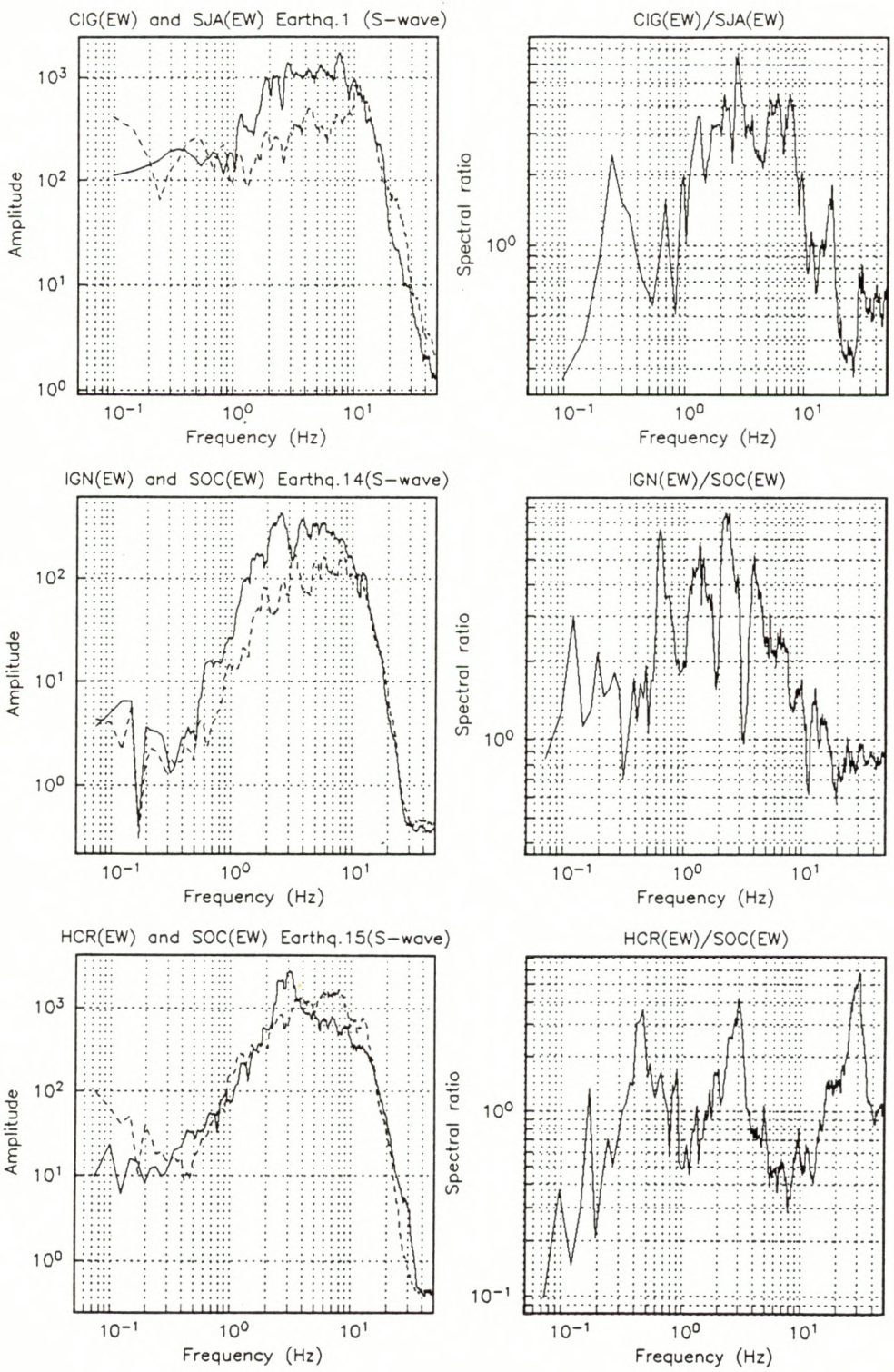
CIG(EW) and SJA(EW) Earthq.1 (S-wave)
CIG(EW)/SJA(EW)
IGN(EW) and SOC(EW) Earthq.14(S-wave)
IGN(EW)/SOC(EW)
HCR(EW) and SOC(EW) Earthq.15(S-wave)
HCR(EW)/SOC(EW)
Amplitude
Spectral ratio
Frequency (Hz)

Figure 13.

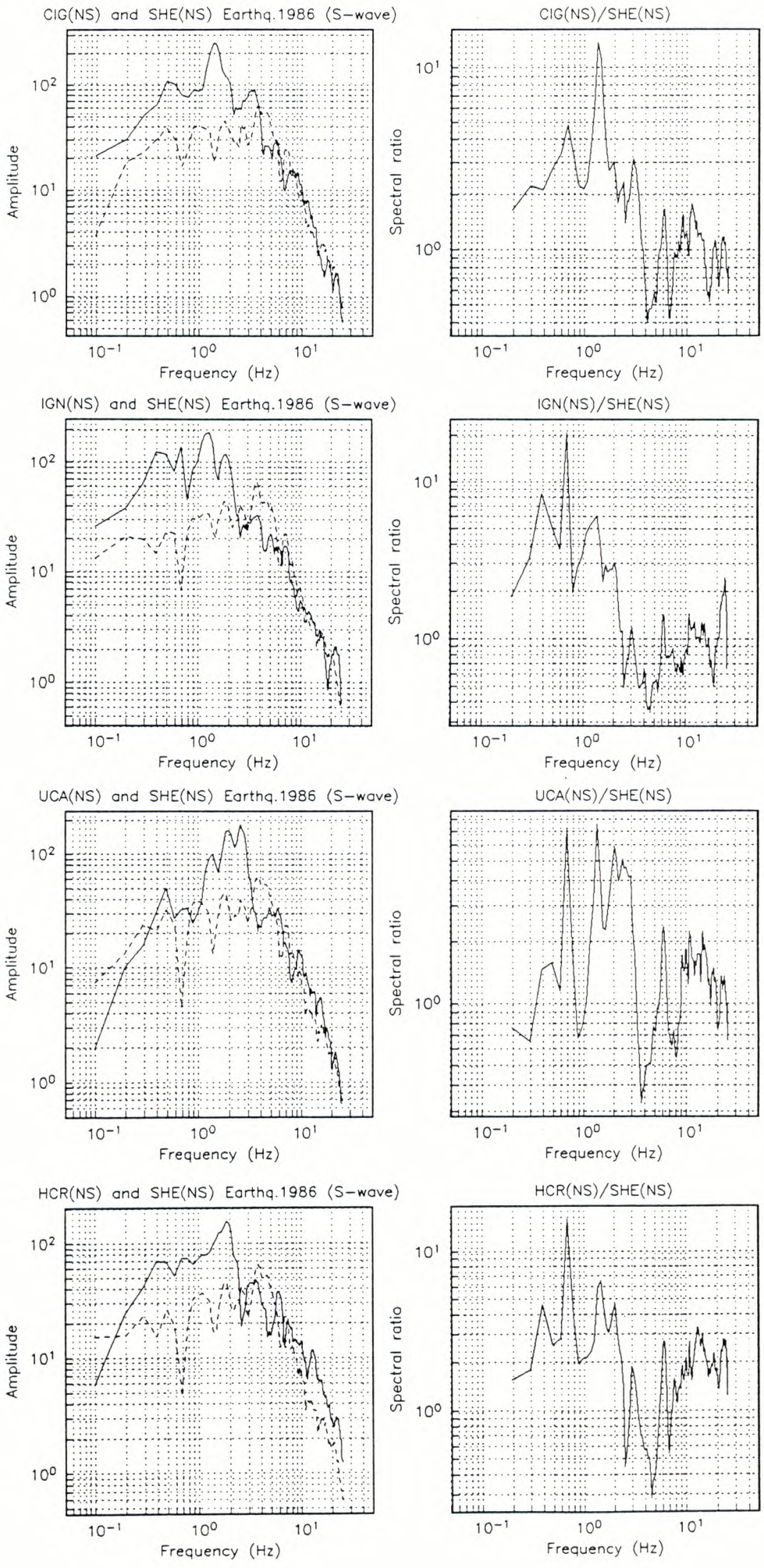
CIG(NS) and SHE(NS) Earthq.1986 (S-wave)
CIG(NS)/SHE(NS)
IGN(NS) and SHE(NS) Earthq.1986 (S-wave)
IGN(NS)/SHE(NS)
UCA(NS) and SHE(NS) Earthq.1986 (S-wave)
UCA(NS)/SHE(NS)
HCR(NS) and SHE(NS) Earthq.1986 (S-wave)
HCR(NS)/SHE(NS)
Amplitude
Spectral ratio
Frequency (Hz)

Figure 14.

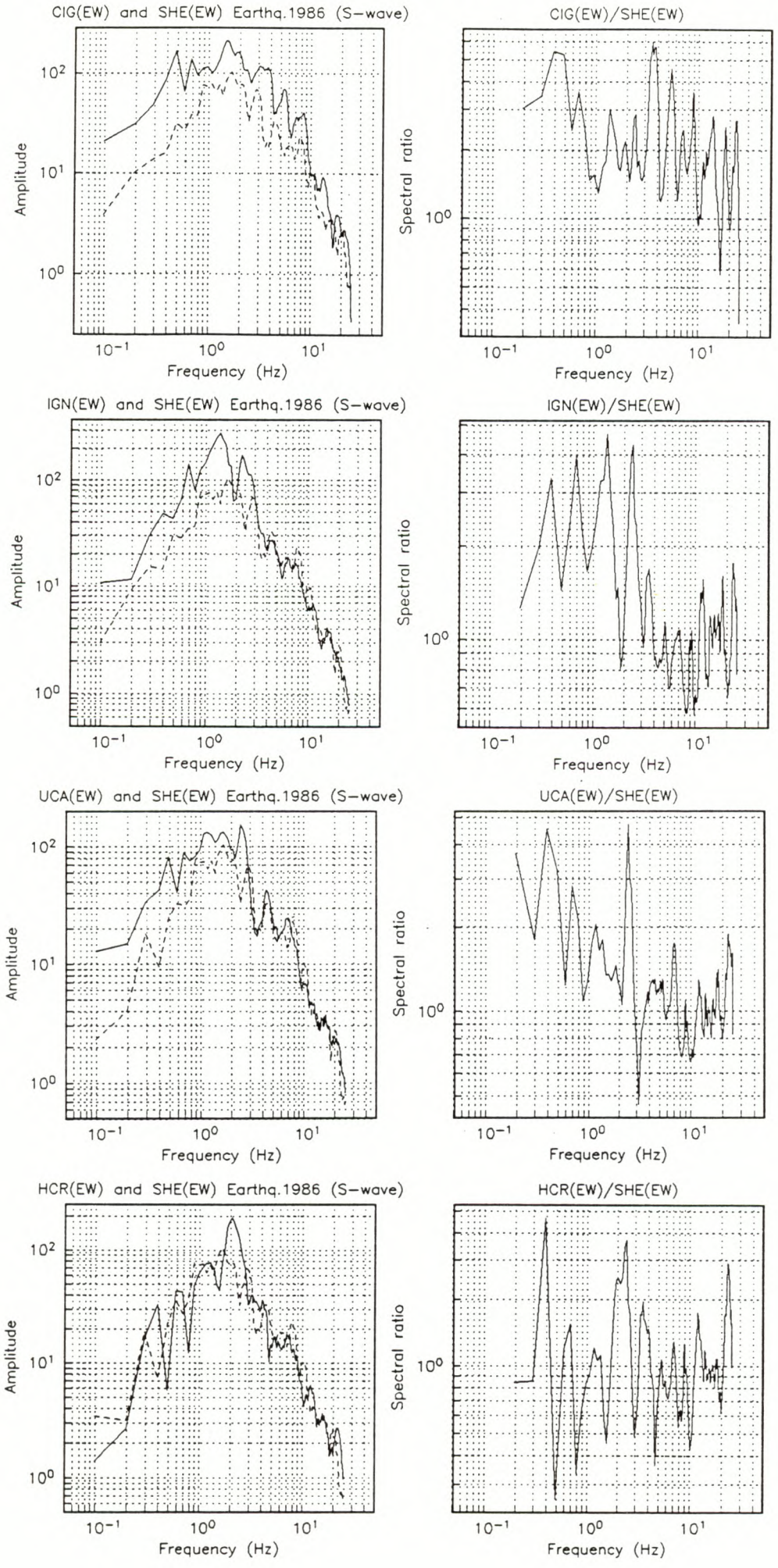
CIG(EW) and SHE(EW) Earthq.1986 (S-wave)
CIG(EW)/SHE(EW)
IGN(EW) and SHE(EW) Earthq.1986 (S-wave)
IGN(EW)/SHE(EW)
UCA(EW) and SHE(EW) Earthq.1986 (S-wave)
UCA(EW)/SHE(EW)
HCR(EW) and SHE(EW) Earthq.1986 (S-wave)
HCR(EW)/SHE(EW)
Amplitude
Spectral ratio
Frequency (Hz)
10^{2}
10^{1}
10^{0}
10^{-1}

Figure 15.

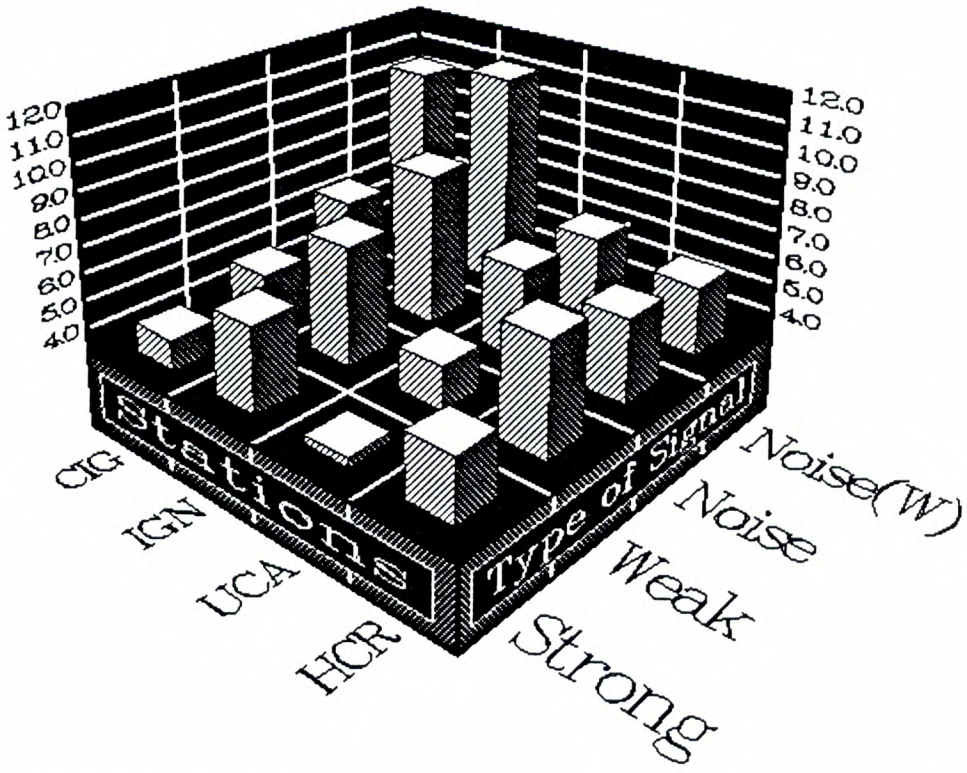

N–S **Average Amplification Factor**

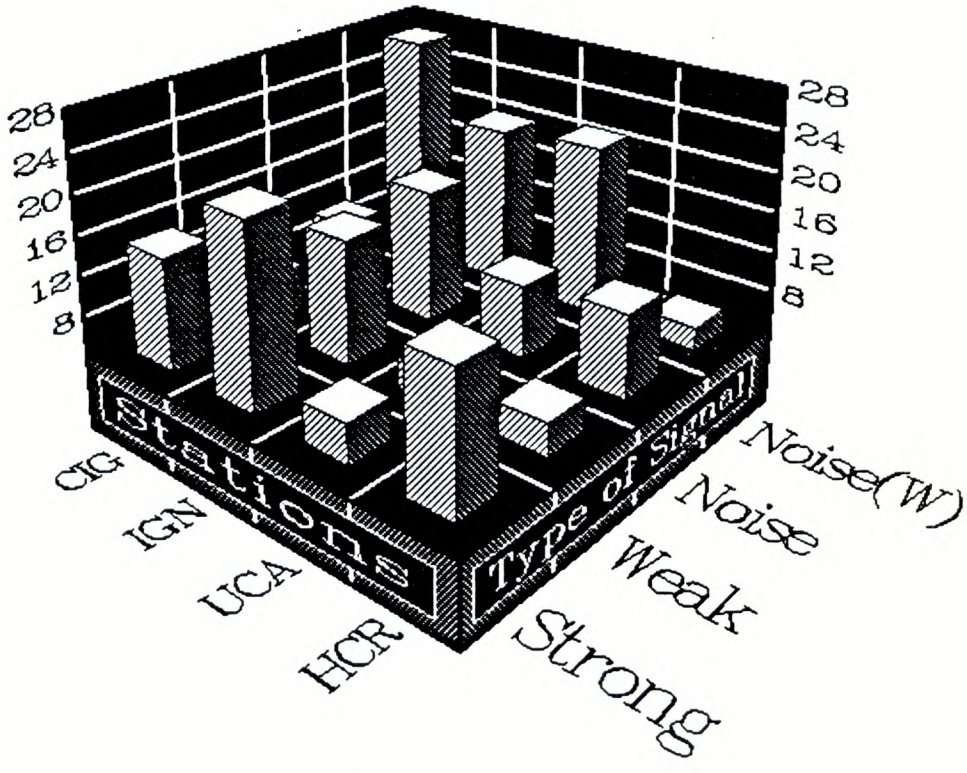

N–S **Maximum Amplification Factor**

Figure 16.

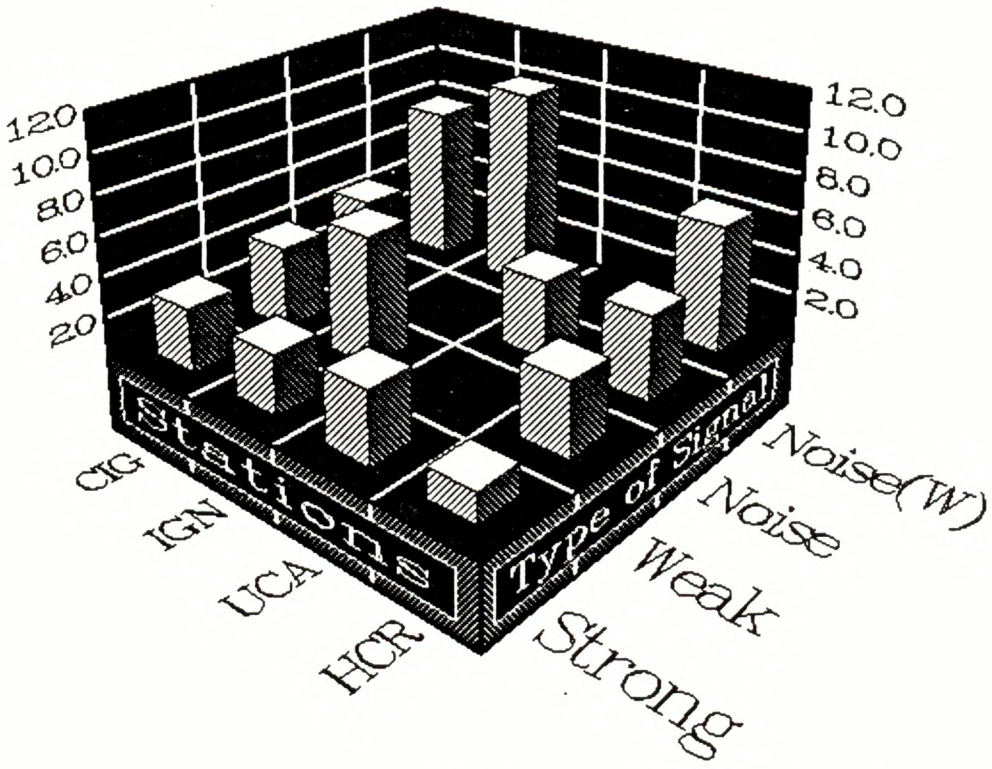

E–W **Average Amplification Factor**

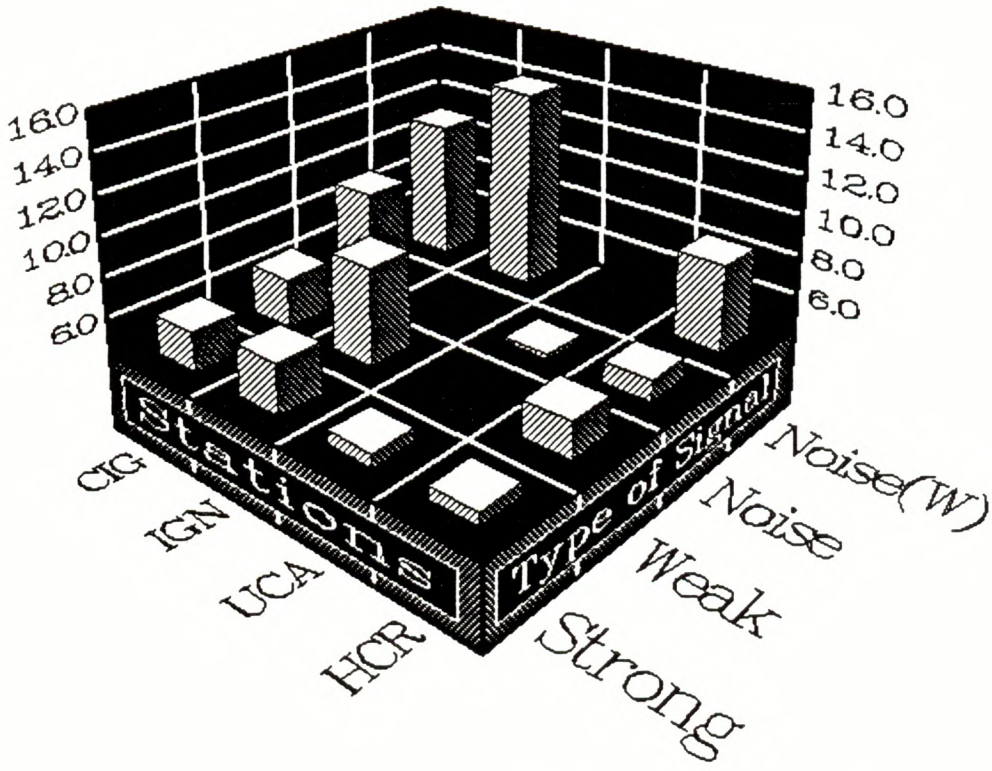

E–W **Maximum Amplification Factor**

Figure 17.

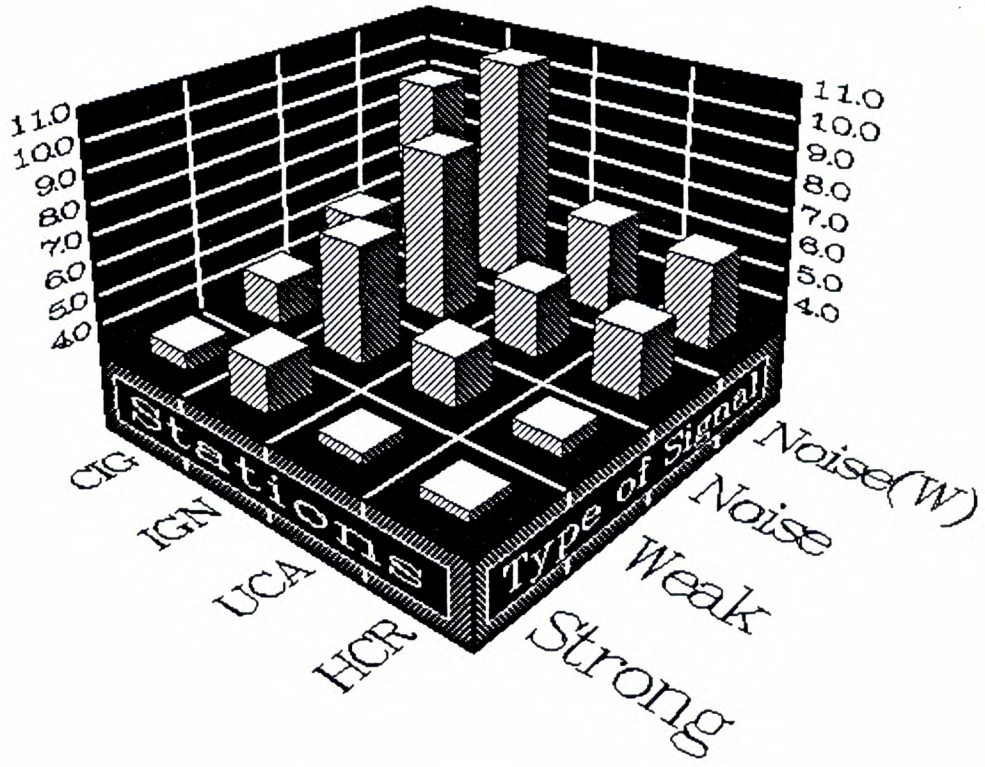

NS–EW **Average Amplification Factor**

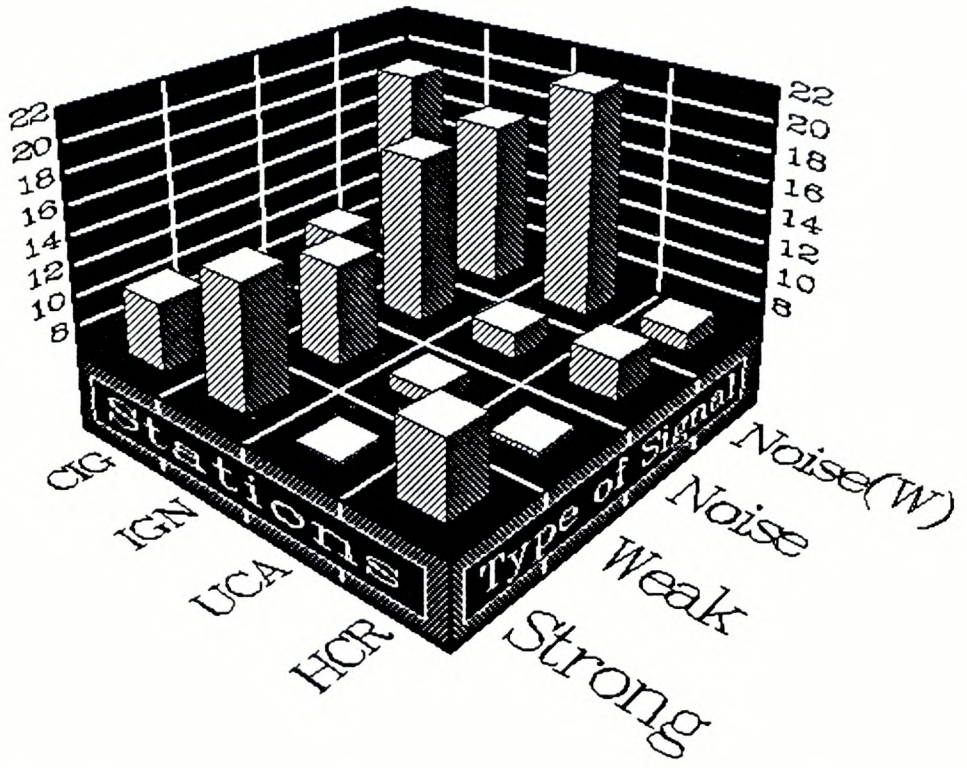

NS–EW **Maximum Amplification Factor**

Figure 18.

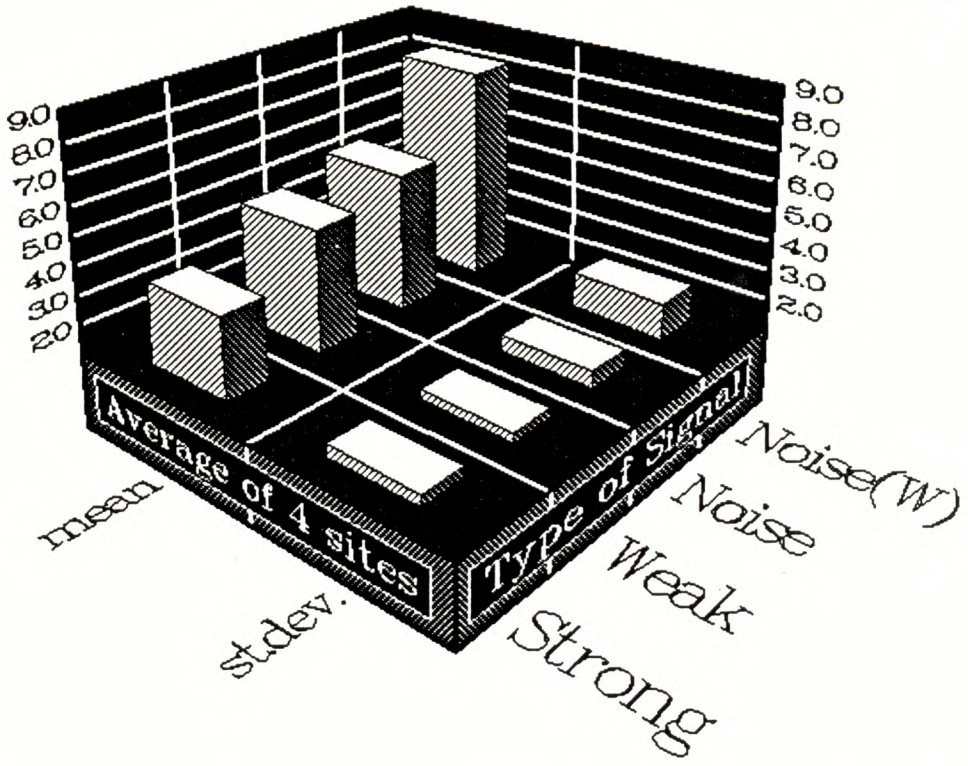

Average **Composite Amplification Factor**

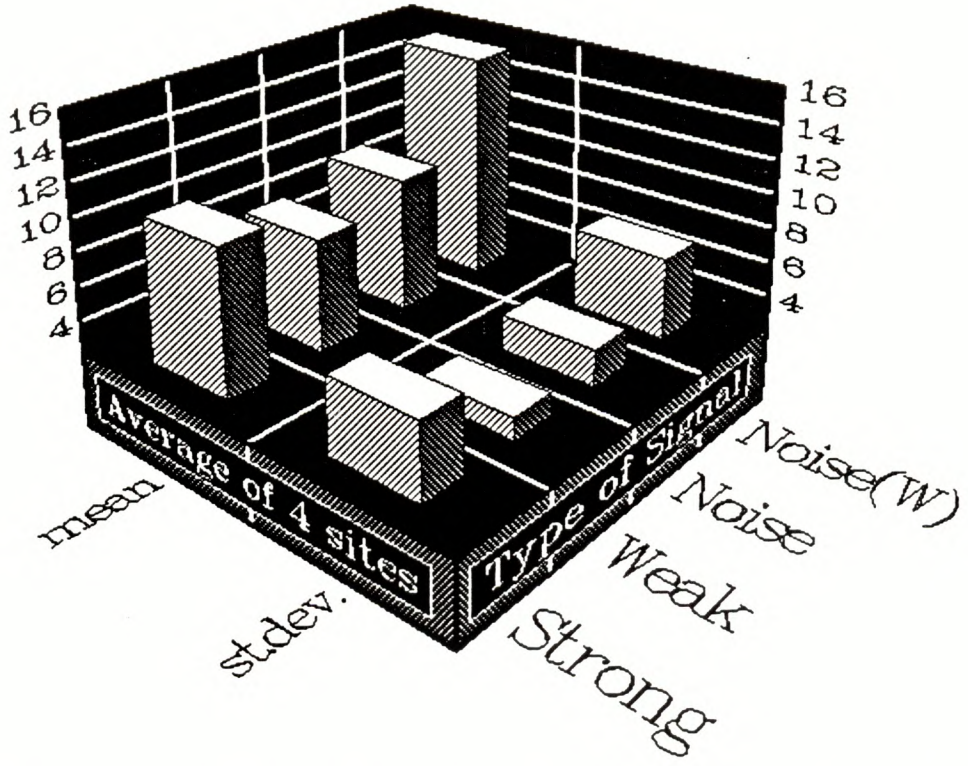

Maximum **Composite Amplification Factor**